Transportation Research Part C 146 (2023) 103960

Contents lists available at ScienceDirect

Transportation Research Part C

journal homepage: www.elsevier.com/locate/trc

Optimal curbside pricing for managing ride-hailing pick-ups and drop-offs

Jiachao Liu [a], Wei Ma [b], Sean Qian [a,c,*]

[a] Department of Civil and Environmental Engineering, Carnegie Mellon University, Pittsburgh, PA 15213, United States of America
[b] Department of Civil and Environmental Engineering, The Hong Kong Polytechnic University, Hong Kong
[c] Heinz College of Public Policy and Information System, Carnegie Mellon University, Pittsburgh, PA 15213, United States of America

ARTICLE INFO

Keywords:
Ride-hailing services
Curbside management
Pick-ups and drop-offs
Multi-modal traffic assignment
Sensitivity analysis
Optimal pricing

ABSTRACT

Recent years have witnessed the rise of ride-hailing mobility services thanks to ubiquitous emerging technologies. Curbside spaces, as a category of public infrastructure, are being used by private ride-hailing services to pick up and drop off passengers, in addition to deliveries and parking access. This becomes quite common in urban areas and has led to additional congestion for ride-hailing, private and public transit vehicles on the driving lanes. Curb utilization by various traffic modes further alters travelers' choices in modes/routes, clogging streets and polluting urban environment. However, there is a lack of theories and models to evaluate the effects of curbside ride-hailing stops in regional networks and to effectively manage ride-hailing pick-ups and drop-offs for system optimum. In view of this, this paper develops a bi-modal network traffic assignment model considering both private driving and ride-hailing modes who are competing for roads and curb spaces in general networks. To model the impact of limited curbside capacity to through traffic, a curbside queuing model is utilized to quantify the effect of congestion on both curbs and driving lanes induced by curbside stops in terms of waiting time and queue lengths. Travelers make joint choices of modes (driving or ride-hailing), curb stopping locations or parking locations. In addition, this study explores the option to regulate the amount of curbside stops to improve system performance, which is done by imposing a location-specific stopping fee on ride-hailing trips for using curbs to pick-up and drop-off. The curb pricing would influence travelers' modal choices and parking location choices. To determine the optimal curbside pricing, a sensitivity analysis-based method is developed to minimize the total social cost of the network among all trips. The proposed methods are examined on three networks. We find that the optimal curbside pricing could effectively reduce curbside congestion and total social cost of the traffic system, benefiting all trips in the network.

1. Introduction

Just like roadways and intersections, curb space is an indispensable part of public infrastructure systems where multi-modal transportation meets, conflicts, and competes for use of limited assets. Emerging mobility technologies prompt explosive usage of curb spaces, as most mobility services and commercial trucks in urban areas need to park at curbs, making curb space unprecedentedly critical. Though roadways and intersections have been extensively studied for decades, very limited efforts have been dedicated to understanding the utilization, occupancy, pricing, and preferred access to curb spaces and the resulting

* Corresponding author at: Department of Civil and Environmental Engineering, Carnegie Mellon University, Pittsburgh, PA 15213, United States of America.
E-mail addresses: jiachaol@andrew.cmu.edu (J. Liu), wei.w.ma@polyu.edu.hk (W. Ma), seanqian@cmu.edu (S. Qian).

https://doi.org/10.1016/j.trc.2022.103960
Received 26 March 2022; Received in revised form 20 July 2022; Accepted 14 November 2022
Available online 5 December 2022

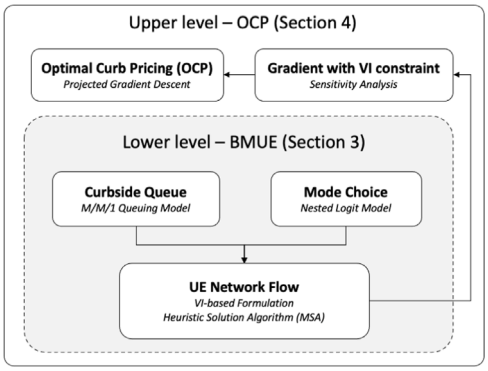

Fig. 1. Framework of this study.

transportation system implications (Shaheen et al., 2019). Evidence shows exponential growth in demand for passenger pick-up/drop-off (PUDO), curbside deliveries, parking, and recent micro-mobility services, and soon to arrive auto-valet service from autonomous vehicles, making curbside spaces more oversaturated and leading to transportation system inefficiency (Castiglione et al., 2016; Li et al., 2016; Castiglione et al., 2018; Agarwal et al., 2019). Therefore, there is a pressing need to analyze the system-level impacts associated with curb usage and manage the scarce curb spaces with the explicit consideration of heightened multi-functional usage.

Ride-hailing (also known as ride-sourcing) services provided by transportation network companies (TNCs), increase user mobility, and offer the flexibility of on-demand PUDO locations, making ride-hailing an active user of curb spaces in urban areas and calling for effective curb management. Meanwhile, it is critical to understand how the operational strategies and policy decisions will change the interactions between different stakeholders of the ride-sourcing platform (Wang and Yang, 2019). Therefore, public agencies are eager to explore options to regulate ride-hailing PUDO, to improve efficiency and sustainability of emerging mobilities.

In view of this, this paper studies curb usage by driving, parking, and ride-hailing vehicles, identifies the potential sources of mobility system inefficiency and proposes strategies of pricing ride-hailing PUDO to improve system efficiency. The optimal pricing strategies are based on the premise of how curb spaces are used by various vehicles with different trip purposes, having substantial impacts on when, where, and how an individual traveler or ride-hailing company makes trips, as well as ripple effects on the entire network.

The content of this paper is organized as follows. Section 2 summarizes related research and addresses research gaps and contributions of our study. Section 3 presents the detailed formulations of the bi-modal traffic assignment model with built-in M/M/1 curbside queuing models, user equilibrium and equivalent variational inequality problem, and the corresponding heuristic solution algorithm. In Section 4, an optimal curb pricing (OCP) strategy which is a bi-level optimization is proposed to manage the curbside PUDO. The upper level is minimizing total social cost for all travelers in the network of study and the lower level is bi-modal user equilibrium (BMUE). Furthermore, a sensitivity analysis-based algorithm is developed to solve the optimization problem and obtain the optimal curb pricing solution. Section 5 examines the proposed framework on a toy network and two real world networks. The effectiveness, efficiency and robustness of the proposed framework are discussed. Lastly, conclusions, potential policy implications and future research directions are drawn in Section 6. The key components of our integrated framework in this study is shown in Fig. 1.

2. Literature review

2.1. Curb operation and management

The operation and management of curbside spaces originate from practical needs. On-street parking in downtown area is a fundamental function of curb spaces and has been studied extensively such as cruising behavior (Geroliminis, 2015; Zheng and Geroliminis, 2016), impact on congestion (Arnott and Inci, 2006, 2010) and dynamic pricing strategies (Qian and Rajagopal, 2014; Pu et al., 2017; Lei and Ouyang, 2017), but few of them considered curb usage of different participants together. Caleb et al. (2021) made a comprehensive review of existing pilot projects of curbside usage and policies, summarizing incoming challenges, demands and opportunities. Since the usage of curbside spaces involves a wide spectrum of stakeholders, the curbside management is usually conceived as achieving a balance for all participants in curbside usage. Several pilot studies have been conducted for different individual components in curbside management, including efforts on commercial loading/unloading (Jones et al., 2009), on-street parking (Millard-Ball et al., 2014) and residential parking (Guo and McDonnell, 2013). There are also studies identifying the supply and demand dynamics with respect to the curbside usage, such as the competitions between curbside parking and downtown garage parking under different parking demands (Arnott and Rowse, 2013; Arnott et al., 2015) and the impacts of regular parking spillovers at popular destinations on curbside usage (Olus Inan et al., 2019). However, early studies on curb management did not capture the

relationship between curb space usage and network traffic dynamics. It was unclear how curb use would impact the traffic flow and thus the system-level network performance.

In recent years, more research has been conducted to build refined models for curbside management strategies, but mostly focusing on single traffic mode. Chen et al. (2016) used agent-based simulation to study the performance of curbside parking and examined if reservation systems outperform come-and-find approaches. Schimek (2018) examined interactions between bikes and curbside, and revealed the fact that there is a strong correlation between bike crashes and parked vehicles on curbs, and further discussed how to design bike-lane/curbside space aiming to reduce bike crashes. On the same topic, Ye et al. (2018) proposed a microscopic examination on the curbside parking to capacity reduction of bike lanes. Goodchild et al. (2019) studied the impact to traffic at destination blocks with dedicated PUDO curbs for TNC services. Riders' different levels of correspondence to this policy was also examined when different measures have been taken to reinforce dedicated curbside PUDOs. Dowling et al. (2020) introduced a network of finite capacity queues to model curbside parking behavior. Patkar and Dhamaniya (2020) studied the impact of curbside bus stops to roadway traffic flow under heterogeneous traffic conditions and found out that curbside bus stops reduce roadway capacity depending on bus arriving rate. Abhishek et al. (2021) developed a queueing network considering both dedicated bays and curbside parking to emphasize the allocation of scarce curbside space. Curb spaces are explosively used by multi-modal travelers which could have interactive effects associated with curb usage. To our best knowledge, few research constructed the multi-modal traffic network models and explored the travel behavior of different modes considering curbside usage.

Analysis on a comprehensive curbside management plan was conducted by Seattle District Department of Transportation (DOT) on the RapidRide Roosevelt Corridor (Zimbabwe, 2018). For the management strategies, the prevailing frameworks included various charging schemes (Jones et al., 2009; Guo and McDonnell, 2013; Millard-Ball et al., 2014; Olus Inan et al., 2019), parking time limits (Arnott and Rowse, 2013), optimal metering rate (Arnott, 2014), dedicated curb spaces for specialized use (Shaheen et al., 2019; Goodchild et al., 2019) and special design of curbside to facilitate special usage (Mccormack et al., 2019; Shaheen et al., 2019). Ugirumurera et al. (2021) developed a micro-simulation based framework to simulate and evaluate curbside traffic managements policies. Most existing research on curbside management policies studied the curbside area solely, and very few work integrated the curbside space into general transportation networks where a complete trip is made or modeled. In fact, different curbside management strategies could significantly affect the travelers' behavior for the entire network and hence may yield considerably different network traffic patterns.

2.2. Ride-hailing services

As a competitive user of curbside spaces emerging explosively recently, ride-hailing services draw tremendous attentions of the transportation research community. On the demand side, Ke et al. (2021) predicted ride-hailing demand for different service options. Wang and Noland (2021) examined the generation of ride-hailing trips by various spatial characteristics, including population density, floor–area ratio, housing prices, road networks, the proximity of public transit, land use mix, and points of interests. On the supply side, Xu et al. (2020) constructed a double-ended queuing model to depict the supply curve of ride-hailing systems under different market conditions. Ride-sharing user equilibrium problems were proposed to model behaviors of drivers (supply) and/or riders(demand), considering different conditions, such as market equilibrium and competition (Di and Ban, 2019; Wang et al., 2021; Ni et al., 2021) and driver–rider matching cost (Chen and Di, 2021). Other related work empirically studied travel characteristics of ride-sourcing drivers and passengers and mode substitution effects (Tirachini and Río, 2019; Acheampong et al., 2020; Urata et al., 2021; Grahn et al., 2021).

Operations of ride-hailing services have also been studied intensively including location prediction of the next rider pick-up (Nair et al., 2020), service matching (Qin et al., 2021) and vehicle rebalancing (Kontou et al., 2020; Guo et al., 2021; Zhu et al., 2022), demand prediction (Battifarano and Qian, 2019), ride reservations (Yahia et al., 2021), impact of expanding service (Beojone and Geroliminis, 2021), shared parking (Gao et al., 2022), and management strategies such as pricing for related parking infrastructure (Liu et al., 2021), service platform (Chen et al., 2021) and market (Zha et al., 2016; Nourinejad and Ramezani, 2020). A macroscopic fluid framework for operating a large-scale on-demand ride-hailing system was developed and used for decision making (Xu et al., 2021). A comprehensive review of the literature on important research problems on ride-sourcing management was conducted by Wang and Yang (2019).

Recently more studies focused on transportation network models considering both ride-hailing and other travel modes, especially the interactions and competitions between ride-hailing services and conventional traffic modes. He and Shen (2015) depicted the transition of taxi services to e-hailing services. Traffic equilibrium models were also developed to model the congestion induced by both personal vehicles and ride-hailing vehicles (Pi et al., 2019; Ban et al., 2019; Xu et al., 2019). Wei et al. (2021) developed a mixed integer nonlinear program framework to optimize transit schedules considering passengers' mode choice between transit and ride-hailing. However, most studies on ride-hailing did not relate the behavior of ride-hailing PUDO to choices of curb spaces. This is the key to success of curbside pricing, as pricing would effectively direct PUDO to most desired streets instead of users' own discretion. This choice is incorporated in our approach.

2.3. Contributions of study

In a nutshell, the research gap lies in modeling behaviors of ride-hailing curbside PUDO (namely the location choice of curbside PUDO) into the multi-modal transportation network. The cost and availability of PUDOs of ride-hailing services can substantially impact the decisions of drivers upon where to stall the vehicle, leading to complex traffic impacts in two-fold: temporary interruption

or blockage of through traffic in urban streets, and impact of riders' decisions on choosing ride-hailing or drive-and-park. Clearly ride-hailing PUDO has substantial impact to the entire transportation network and travelers' behavior. How to manage those PUDOs, particularly discouraging usage of a fraction of scarce, but popular, curb spaces through an economic instrument, may help effectively improve transportation system efficiency. This is the intuition to develop this study.

In this paper, we model the curbside space usage by ride-hailing services and the effects of curbside pricing on those ride-hailing services to network-wise congestion patterns. A higher portion of trips in the network using ride-hailing vehicles, leads to more curbside stops to PUDO passengers. The increasing number of PUDOs could saturate the limited curbside public spaces, and potentially generate extra travel delays for both riders and through traffic. For example, if many ride-hailing vehicles choose to PUDO passengers at the same curbside location, it could cause extra congestion at that location due to limited space. When the number of expected stops exceeds the capacity of the curbside space, vehicles waiting to stop at the curbside could spill over to main road, causing delay to the through link flow in the network.

In view of this, a novel bi-modal traffic assignment model is proposed considering the effects of ride-hailing curbside PUDO on congestion. The effects of curbside space usage to PUDO and through traffic are explicitly modeled through a M/M/1 queue. The cost and availability of curb space use are embedded in the utility function that governs the location choices of ride-hailing services, as well as the mode choices of travelers. An optimal curb pricing strategy is designed to regulate temporary stops of ride-hailing at curbs in order to minimize the system-level social costs. The main contributions of this paper are summarized as follows:

- **This study develops a bi-modal user equilibrium (BMUE) model considering two travel modes: driving and ride-hailing, in a general transportation network.** Trips in the network are made to areas with limited curbside spaces that can be used for on-street parking if driving, or for passenger PUDOs if ride-hailing. Generally, these two modes would compete for limited curb spaces, and congestion near/on curbside can further impact the mode choice during the modeling time period. The proposed BMUE model enables the study of a travel mode choice and shift of demand between these two competitive modes when primary factors influencing travelers' decisions include time/cost of driving, parking, ride-hailing, and PUDOs. Therefore, curb pricing can be leveraged to influence travelers' choices on where to park or PUDO. It also offers a holistic approach to assess how travelers' mode choice will be changed and how driving and system-level performance will be impacted when we implement ride-hailing PUDO regulations. We also model the choices of curb PUDO locations (upon the choice of ride-hailing) and parking locations (upon the choice of driving) in the BMUE. Generally, BMUE can also model the competition of two modes for limited curb space if drivers are permitted to use the curb space for on-street parking, which can further impact the mode choices of travelers.
- **This study integrates a curbside queuing model into the equilibrium model to encapsulate the network traffic effect of curbside stopping.** The queuing model allows the network flow model to capture traffic impacts of the increasing number of ride-hailing PUDO demands, which is being observed in many metropolitan areas (Henao and Marshall, 2019; Erhardt et al., 2019; Brown, 2022). More ride-hailing demands will result in an increasing number of curbside stops and potentially additional congestion due to the limited capacity of curbside spaces. The metrics of curb PUDO congestion are imbedded in the utility functions of two modes of interest and further impact the mode choice, PUDO location choice of ride-hailing and parking location choice of driving.
- **This study analytically develops an optimal curbside pricing strategy for curbside management and examines the OCP framework on different networks including a real-world sizeable network, Pittsburgh regional network.** We propose to use optimal curbside pricing to manage the ride-hailing PUDOs at curbs. A sensitivity analysis-based approach is developed to solve for the optimal curbside pricing. The numerical experiments demonstrate the feasibility of proposed model and algorithm in large-scale networks and derive location-specific curbside management policies for real-world applications. Additionally, how OCP can be coupled with potential policy and strategic decisions is also discussed.

3. Bi-modal user equilibrium (BMUE)

This section presents detailed formulation of the BMUE model. First, a M/M/1 queue model is used to model the congestion caused by ride-hailing vehicles stopping at a curb with limited spaces and a nested logit model is used to model travelers' choice behaviors in routes, modes, driving parking locations and ride-hailing PUDO locations. Then the BMUE model is reformulated as an equivalent Variational Inequality (VI) problem. Finally, a heuristic solution algorithm is developed to solve the BMUE. Constants and variables used throughout this paper are summarized in Table 1.

3.1. Network setup

Consider a general transportation network represented by $G = (N, A)$, where N and A are node and link set respectively. During the commute time T, for each origin–destination node pair (r, s) where $r \in R, s \in S$ and $R, S \subseteq N$, there are totally q^{rs} travelers heading to node s from node r. Travel behavior is characterized by modal choice (driving or ride-hailing), route choice, and parking location choice (upon driving) or PUDO location choice (upon ride-hailing). For travelers choosing driving mode, they have the choice of where to park which is called parking location choice throughout our study. There are three options: (1) parking right at the destination parking facility where no walking to destination is needed; (2) parking on-street which competes with those curb spaces for ride-hailing vehicle PUDOs; or (3) parking at off-street parking spaces accessible from a link. For travelers choosing the ride-hailing mode, they make choice of where to be picked up and dropped off, which is called PUDO location choice throughout

Table 1
Notation list.

G	The network.
N	The set of all nodes.
A	The set of all links.
G'	The expanded network when curb nodes split the links.
N'	The set of all nodes in the expanded network.
A'	The set of all links in the expanded network.
R	The set of all origins, $R \subset N$.
S	The set of all destinations, $S \subset N$.
N_v	The vicinity set for a node $v \in N$.
N_v^f	The feasible vicinity set for a node $v \in N$ that are within ζ_v.
K_D^{rs}	The set of all driving paths connecting r to s with $r \in R$ and $s \in S$.
K_R^{rs}	The set of all ride-hailing paths connecting r to s with $r \in R$ and $s \in S$.
ζ_v	Maximum walking distance to generate feasible vicinity of node v.
κ_a	A parameter related to curbside capacity of link a.
α	A parameter representing the value of time.
μ_m	Cost of driving per mile.
T	Total duration of the morning commute.
t_c	Average time for vehicles to complete curbside stops
α_D	Parameter for the driving mode in the Logit model.
α_R	Parameter for the ride-hailing mode in the Logit model.
β	Parameter in the Logit model.
ϵ	A parameter to regulate queuing models.
η_a	Coefficient in the activation function $\Omega_a(\cdot)$.
ω	A threshold for piece-wise linear function used as $\Omega_a(\cdot)$.
q^{rs}	Total OD demand from $r \in R$ to $s \in S$.
q_D^{rs}	The OD demand via driving from $r \in R$ to $s \in S$.
q_R^{rs}	The OD demand via ride-hailing services from $r \in R$ to $s \in S$.
x_a	Link flow on link $a \in A$.
p_a	The number of pick-up/drop-off stops made at curbside of link $a \in A$.
l_a	Length of link $a \in A$
C_a	Flow capacity of link $a \in A$
$t_{\mathrm{ff}a}$	The free flow travel time of link $a \in A$
$\lambda_{a,1}$	Arrival rate of curbside of link $a \in A$
$\lambda_{a,2}$	Service rate of curbside of link $a \in A$
v_a	Average queuing length at link $a \in A$.
w_a	Average waiting time at link $a \in A$.
a_k	The link that path k ends at.
$\delta_a^{rs,k}$	Indicator variable, $\delta_a^{rs,k} = 1$ if $a \in A$ is in path $k \in K_D^{rs}$, $\delta_a^{rs,k} = 0$ otherwise.
$\sigma_a^{rs,k}$	Indicator variable, $\sigma_a^{rs,k} = 1$ if $a \in A$ is in path $k \in K_R^{rs}$, $\sigma_a^{rs,k} = 0$ otherwise
$\gamma_a^{rs,k}$	Indicator variable, $\gamma_a^{rs,k} = 1$ if path $k \in K_R^{rs}$ starts or ends in $a \in A$, $\gamma_a^{rs,k} = 0$ otherwise.
$l_{\mathcal{M}}^{rs,k}$	The length of path k, where $k \in K_{\mathcal{M}}^{rs}$ for $\mathcal{M}$ be $\mathcal{D}$ or $\mathcal{R}$.
μ_s	The parking cost for driving mode for going to destination $s \in S$.
$c_D^{rs,k}$	Travel cost for driving from $r \in R$ to $s \in S$ via path $k \in K_D^{rs}$.
$c_R^{rs,k}$	Travel cost for ride-hailing from $r \in R$ to $s \in S$ via path $k \in K_R^{rs}$.
$\mu_w^{rs,k}$	The walking cost for path $k \in K_R^{rs}$ when using the ride-hailing services.
$f_D^{rs,k}$	Path flow on path $k \in K_D^{rs}$.
$f_R^{rs,k}$	Path flow on path $k \in K_R^{rs}$.
μ_D^{rs}	Equilibrium cost for driving between $r \in R$ and $s \in S$. $\mu_D^{rs} = \min_{k \in K_D^{rs}} c_D^{rs,k}$
μ_R^{rs}	Equilibrium cost for ride-hailing between $r \in R$ and $s \in S$. $\mu_R^{rs} = \min_{k \in K_R^{rs}} c_R^{rs,k}$
$\theta_{a,D}^{rs,k}$	factor indicating the length fraction of link a to be used in the driving path k between OD pair rs.
$\theta_{a,R}^{rs,k}$	factor indicating the length fraction of link a to be used in the ride-hailing path k between OD pair rs.
$\tau_a^{rs,k}$	Indicator variable, $\tau_a^{rs,k} = 1$ if the driving path k ends at a curb node and 0 otherwise
$\Phi_a(\cdot)$	The link performance function of link $a \in A$.
$\Psi(t, l)$	The cost function for ride-hailing trip with duration t and traveled distance l.
$\Omega_a(\cdot)$	User-specified activation function for link $a \in A$.

(*continued on next page*)

this paper. Ride-hailing users first walk to a pick-up curb, ride on the service vehicle, arrive at the drop-off curb, and finally walk to the destination. We assume all travelers are fully aware of the network traffic conditions and behave rationally following classical User Equilibrium. Those choices are governed by a nested logit model which is discussed in detail in Section 3.3. In this study, we assume the demand q_{rs} is fixed and exogenous. It can be estimated based on typical planning models or real-world data. There exist a number of studies to estimate origin–destination demand using data, and comprehensive reviews can be found in Castillo et al. (2015), Ma and Qian (2018) and Ma et al. (2020).

An illustrative example of the parking choice for the two modes is shown in Fig. 2. For a traveler who chooses driving, he/she has three options to park the car before arriving at the destination: (a) destination parking, meaning parking directly at the destination. Each destination has a destination parking facility attached. This option is shown as driving route 1, starting from O, parking at DP,

Table 1 (*continued*).

$\mathbf{x}$	Vector of link flow $\{x_a\}$, $\forall a \in A$
$\mathbf{f}$	Vector of path flow $\{f_{\mathcal{M}}^{rs,k}\}$, $\forall r \in R, s \in S, k \in K_{\mathcal{M}}^{rs}$
$\mathbf{p}$	Vector of pick-up/drop-off stops made at curbsides $\{p_a\}$, $\forall a \in A$
λ_1	Vector of arrival rate of curbsides $\{\lambda_{a,1}\}$, $\forall a \in A$
λ_2	Vector of service rate of curbsides $\{\lambda_{a,2}\}$, $\forall a \in A$
$\mathbf{v}$	Vector of average queuing time at curbside $\{v_a\}$, $\forall a \in A$
$\mathbf{m}$	Vector of curb price μ_a, $\forall a \in A$
$\mathbf{w}$	Vector of average waiting time at curbsides $\{w_a\}$, $\forall a \in A$
$\mathbf{c}$	Vector of path cost $\{c_{\mathcal{M}}^{rs,k}\}$, $\forall r \in R, s \in S, k \in K_{\mathcal{M}}^{rs}$
$\mathbf{c}_*$	Vector of generalized path cost $\{c_{*\mathcal{M}}^{rs,k}\}, \forall r \in R, s \in S, k \in K_{\mathcal{M}}^{rs}$
$\mathbf{q}$	Vector of O-D demand $\{q^{rs}\}$, $\forall r \in R, s \in S$
Δ	Link-path indicator matrix $\{\delta_a^{rs,k}\}$, $\forall r \in R, s \in S, k \in K_{\mathcal{M}}^{rs}$
Λ	Path-demand indicator matrix $\{\sigma_a^{rs,k}\}$, $\forall r \in R, s \in S, k \in K_{\mathcal{M}}^{rs}$
Γ	Ride-hailing path-end link indicator matrix $\{\gamma_a^{rs,k}\}$, $\forall r \in R, s \in S, k \in K_{\mathcal{M}}^{rs}$

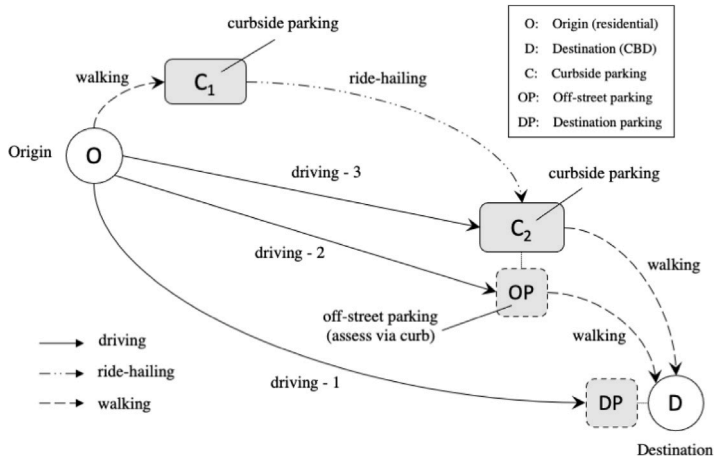

Fig. 2. An illustrative example of parking choice.

which is connected with the destination by a dashed line, meaning they are at same location; (b) curbside parking, meaning parking at a curbside space which might compete for the limited space with ride-hailing vehicles, shown as driving route 3 in the figure, starting from O, parking at C_2 and walking to destination D; (c) off-street parking via curb, meaning parking at off-street facility which is closed to and accessible through curbside space. If the traveler chooses this option, the vehicle will not participate in the curb queue. This parking option is shown as driving route 2 starting from O, parking at OP, and walking from OP to destination D. For simplification, we consider the off-street parking facility and curbside space are exactly at same location (i.e. C_2 and OP are connected with dashed line meaning they are at same location). As a result, option 2 and 3 can be combined in our study.

A route for a traveler choosing ride-hailing consists of three parts: (a) walking from origin to a curb location to be picked up, (b) transferred by the ride-hailing vehicle from the pick-up curb location to another curb location to be dropped off, (c) walking from the drop-off curb location to destination. For a ride-hailing route, PUDO location choice will be considered. In the figure, an arbitrary ride-hailing route is starting from node O, walking to curbside parking node C_1, traveling from C_1 to C_2 and walking from C_2 to destination D.

Based on the setting above, we extend the network to accommodate the parking options for two modes. Each destination node $s \in S$ has a parking lot with unlimited capacity hence private vehicle travelers can park there regardless of the parking demand. To model PUDO behavior at curbside space and private vehicle parking choice, a curb node is introduced for each link $a \in A$ in the network. At each curb node, there exist both a limited curb space for ride-hailing vehicles to stop temporarily and unlimited parking space, on-street or off-street, for private vehicles to park. Therefore, each curb node represents both PUDO locations for ride-hailing and a collection of parking spaces for driving. Since the curb space has a limited capacity, there could be congestion when ride-hailing vehicles demand is high, leading to queue spilling over to driving lanes. However, for private vehicles, all of them can park at those spaces connected to the curb node, and once they enter the curb node, they are assumed to have no contribution to the roadway congestion. In addition, no parking cruising is assumed in the context of day-to-day network equilibrium. More details will be discussed in next Section 3.2.

For a node $v \in N$, a vicinity N_v is defined as the set of curb nodes around node v within a walking distance of ζ_v along the feasible paths between curb nodes and v. However, due to possible restrictions for parking or PUDO, not all curb nodes are allowed to park or access, therefore a feasible vicinity N_v^f of node v is defined as the set of curb nodes allowed to park or access in the vicinity set N_v. N_v^f represents a collection of possible choices of parking or curbside PUDO locations for each node $v \in N$.

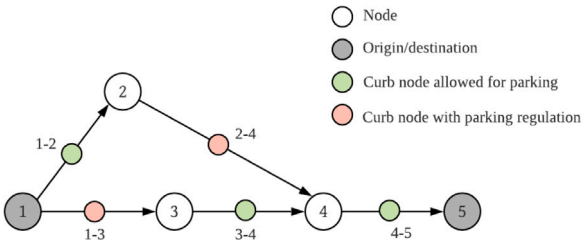

Fig. 3. An illustrative example of network setup. (For interpretation of the references to color in this figure legend, the reader is referred to the web version of this article.)

For each origin–destination node pair (r, s) where $r \in R, s \in S$ and $R, S \subseteq N$, there are two path sets, one for each mode: driving path set K_D^{rs} and ride-hailing path set K_R^{rs}. Separate rules are defined for generating feasible paths for driving and ride-hailing, respectively. For a driving path $k_D \in K_D^{rs}$, its start node must be an origin node r, while its end node can be either a destination node s (park right at the destination) or those curb nodes in the set N_s^f (parking off-street or on-street, then walk to the destination). This implies the choice of an end node depends on parking location choice. Quite differently, for a ride-hailing path $k_R \in K_R^{rs}$, both the start and end nodes must be curb nodes which are in the feasible vicinities of origin and destination nodes, denoted by sets N_r^f and N_s^f respectively. This implies ride-hailing vehicles can only pick up and drop off passengers at the curbside. If a traveler want to call a ride-hailing service, he/she must walk to one of the feasible pick-up curb locations in the vicinity of the origin, take ride-hailing vehicles, be dropped off at one of the feasible curb locations near the destination, and finally walk to the destination. Therefore, ride-hailing travelers have PUDO location choices among all feasible curb locations.

A simple example is given to better illustrate this setup in Fig. 3. The network only has 1 OD pair (1,5) and 5 links. The length of link 1-2, 1-3, 3-4 and 4-5 are all 1 mile each and link 2-4 is 2 miles. All curb nodes are assumed to be half way of each link and denoted as the corresponding link id. Due to parking regulation, only curb nodes 1-2, 3-4 and 4-5 (green nodes) are allowed for parking and PUDO. Set the walking threshold $\zeta_1 = \zeta_5 = 0.5$ mile, then we have the feasible vicinity of origin node 1 is {1-2} and the feasible vicinity of destination node 5 is {4-5}. Thus we can generate 4 paths for driving: path $1 \to 2 \to 4 \to 5$, path $1 \to 3 \to 4 \to 5$, path $1 \to 2 \to 4 \to$ 4-5, and path $1 \to 3 \to 4 \to$ 4-5. The former two paths start from origin node 1 and park at destination node 5, while the latter two paths end at curb node 4-5 indicating that the travelers choose to park at or near the curb and walk to destination. There is only one path for the ride-hailing mode, path 1-2 $\to 2 \to 4 \to$ 4-5, which starts and ends at feasible curb nodes. In this example, driving mode can choose to park off-street/on street at curb node 4-5 or at destination parking facility 5. The choice depends on the curb congestion occurred at the curb node 4-5. If a number of ride-hailing vehicles need to park at the curb 4-5 and causing a large delay for the link 4-5, then it could avoid half of the large driving time on the link if parking at 4-5 and walking to destination. But it really depends on the severity of curb congestion and whether the half of driving time on link is larger than walking to destination. Different options for parking are provided in our study and travelers can make choices based on travel cost.

3.2. Modeling curbside stops

When excessive ride-hailing vehicles stop at the same curb, the curb will be congested due to the limited capacity, and the impact to the network will be two-fold: (1) picking up or dropping off a ride-hailing traveler will take more time as a result of queuing ride-hailing vehicles; and (2) severe curb congestion can spill over to the driving lanes and thus affect the through traffic. The impact will change both the cost of curbside parking/stops and roadway travel time, further inducing the change in travelers' behavior in choosing routes and/or modes, and subsequently the network performance. Therefore, the effects of curbside stops should be incorporated in the traffic network models.

In this paper, each curb in the network is treated as a single server with limited service slots processing curbside parking/stops. We assume the curbside stops follow a randomized queuing process over the entire commuting period T. The classic M/M/1 queue model can be used to depict the queue formed at the curb node for each link $a \in A$. The reason we choose M/M/1 model is two-folds. Firstly, M/M/1 model has simple analytical formulas of metrics without sacrificing the realism as much. In Section 4 sensitivity analysis based method is developed to analytically determine the optimal curb pricing and the derivative of queue metrics with respect to arrival rate is needed when calculating derivative of objective function with respect to the curb pricing. The M/M/1 metrics are analytically differentiable with respect to the arrival rate in a closed form. On the other hand, M/M/1 can capture the main characteristics of the curb usage. The curbside can be seen as a service site where the number of curb spaces is limited to serve PUDOs, and vehicle arrivals in traffic engineering theory are often treated to follow an exponential distribution. If we assume the curb usage time also follows an exponential distribution, then the curb queue can be approximated by M/M/1. The expected queue length and waiting time in queue can be obtained analytically. Although we choose the simple M/M/1 model in our study, our framework is compatible with any other queuing models. The congestion related metrics, namely the queue length and waiting time terms in the generalized cost formulas, can be associated with any queuing model of choice.

Based on our setting, only ride-hailing PUDOs can form queues at curb space and may have effect on through traffic depending on the queue characteristics, while private vehicles parked curbside or off-street do not contribute to the curbside queues potentially

spilling over to the driving lanes. Hence the curb queue is only related to arrival numbers of ride-hailing PUDOs. During the commuting period T, the number of curbside stops made at link $a \in A$ is denoted as p_a, as presented in Eq. (1).

$$p_a = \sum_{r \in R} \sum_{s \in S} \sum_{k \in K_{\mathcal{R}}^{rs}} f_{\mathcal{R}}^{rs,k} \gamma_a^{rs,k} \tag{1}$$

where $f_{\mathcal{R}}^{rs,k}$ is the ride-hailing flow for path k connecting OD pair rs; $\gamma_a^{rs,k}$ is an indicator variable and equals to 1 if path $k \in K_{\mathcal{R}}^{rs}$ either starts or ends in $a \in A$ or 0 otherwise. The M/M/1 model has two assumptions which can be utilized to derive closed-form characteristics of the queueing system.

Assumption 1. The time gap between each two consecutive arrivals of the p_a vehicles is exponentially distributed with parameter $\lambda_{a,1}$, computed in Eq. (2), during the entire commute time T.

$$\lambda_{a,1} = \left(\frac{T}{p_a} \right)^{-1} \tag{2}$$

$\lambda_{a,1}$ is exactly the arrival rate used in M/M/1 model. Our assumption is that, on average, the ride-hailing vehicle stops follow the same pattern across the entire commuting period T. This is consistent with the general assumption of static traffic assignment (STA) models for the morning peak hour.

Assumption 2. The time for a ride-hailing vehicle to complete a curbside stop, namely the duration of a PUDO, is exponentially distributed with parameter $\lambda_{a,2}$, as presented in Eq. (3), during the entire commute time T.

$$\lambda_{a,2} = \left(\frac{t_c}{\kappa_a \cdot l_a} \right)^{-1} \tag{3}$$

where t_c is average time needed for ride-hailing vehicles to complete curbside stops; κ_a is the curb capacity density of link a and $\kappa_a \cdot l_a$ gives the capacity of the curbside for ride-hailing vehicle stops on link a.

$\lambda_{a,2}$ is also known as service rate and the expected curbside stop duration is $\frac{t_c}{\kappa_a \cdot l_a}$. Since we use a M/M/1 whereas the curbside allows multiple stops at the same time, the expected curbside stop time has a denominator $\kappa_a \cdot l_a$, which is the capacity of the curb space for each link a. In this paper, the curb capacity density κ_a is fixed meaning curb capacity is exogenous to the transportation system and independent of traffic flow. So that the number of ride-hailing vehicles a curb space can serve is fixed. The capacity of each curb can be predetermined based on historical observations. In future study, we plan to make curb capacity endogenous to model competition between ride-hailing and private vehicles to use the limited curb space.

Both parameters of the M/M/1 queue model are considered in expectations and not time-varying within the time slot of study since the BMUE is a STA problem. Based on the M/M/1 queuing theory, two queuing metrics can be derived, expected queuing length at the curb v_a and expected waiting time before completing a curb stop w_a, as presented in Eq. (4).

$$\begin{aligned} v_a &= \frac{\lambda_{a,1}/\lambda_{a,2}}{1 - \lambda_{a,1}/\lambda_{a,2}} = \frac{\lambda_{a,1}}{\lambda_{a,2} - \lambda_{a,1}} \\ w_a &= \frac{1}{\lambda_{a,2} - \lambda_{a,1}} \end{aligned} \tag{4}$$

Remark 1. Both metrics will be integrated in the generalized path costs for two modes. The expected queuing length v_a determines the amount of spillover to driving lanes. This spillover may cause additional delay for both driving and ride-hailing vehicles using these driving lanes. The additional delay term $\Omega(v_a)$ for link a is added to Eq. (6) indicating there will be some additional travel time if spillover occurs at the curb of link a. The average waiting time w_a can be interpreted as the total time a ride-hailing vehicle spending in the curbside queue of link a, namely the total waiting time to access curb of link a and complete parking for pick-up or drop-off.

Remark 2. The classic M/M/1 model assumes $\lambda_{a,1} < \lambda_{a,2}$ and otherwise the derivation of v_a and w_a would become meaningless. But this assumption is not guaranteed in our model: in extreme cases, more vehicles could arrive at the same curb than the curb capacity allows. In this scenario, the queue should have long waiting time and queuing length. To accommodate this condition in our model, we modify the expressions for v_a and w_a in Eq. (5) by adding a threshold ϵ. Eq. (5) approximates the curbside queue when an excessive number of vehicles arrives for curbside stops.

$$\begin{aligned} v_a &= \frac{\lambda_{a,1}}{\max(\epsilon, \lambda_{a,2} - \lambda_{a,1})} \\ w_a &= \frac{1}{\max(\epsilon, \lambda_{a,2} - \lambda_{a,1})} \end{aligned} \tag{5}$$

where ϵ is a user-specified small value that regulates the value of v_a and w_a once $\lambda_{a,1}$ is equal or greater than $\lambda_{a,2}$. A sufficient large waiting time and queue length would dis-encourage ride-hailing vehicles to use this specific link for stops.

3.3. User equilibrium

This section shows the formulation of the BMUE model. First, two generalized path cost functions are defined for driving and ride-hailing, respectively, in Eq. (6). The path cost for driving vehicles $c_D^{rs,k}$ consists of four terms: (1) travel time cost, (2) fuel cost, (3) parking fee and (4) potential walking cost (if parking off-street or on-street). Both travel time cost and fuel cost are associated with each path, whereas the parking fee is assumed to be associated with the parking facility used. Since the focus of this study is to understand the impact of curbside pricing that varies by each link, we approximate the parking fee with a destination-specific constant, representing an expected fee to pay for parking at or near a particular destination. $\tau^{rs,k}$ is a 0-1 indicator variable and equals to 1 if the driving path k ends at a curb node, then a walking cost term $\mu_w^{rs,k}$ is added in the path cost.

While the path cost for ride-hailing vehicles $c_R^{rs,k}$ consists of four terms: (1) travel time cost, (2) ride-hailing service fee, (3) walking cost; and (4) additional waiting time cost due to curbside queues. For ride-hailing trips, we assume the ride-hailing service fee Ψ depends on both travel time and travel distance. Note that when calculating the travel time cost for driving and ride-hailing, link-level travel time includes a term $\Omega(v_a)$ indicating the curbside queue's effect on the through traffic on driving lanes is considered. Here we assume the system is passenger-uncongested and passengers do not have additional wait time for ride-hailing vehicles to arrive.

$$\begin{cases} c_D^{rs,k} = \alpha \sum_{a\in A'} \left(\Phi_a(x_a) + \Omega_a(v_a)\right) \delta_a^{rs,k} + \mu_m l_D^{rs,k} + \mu_s + \mu_w^{rs,k} \tau^{rs,k} \\ c_R^{rs,k} = \alpha \sum_{a\in A'} \left[\left(\Phi_a(x_a) + \Omega_a(v_a)\right) \sigma_a^{rs,k} + \gamma_a^{rs,k} w_a\right] + \Psi\left(\sum_{a\in A'} \left(\Phi_a(x_a) + \Omega_a(v_a)\right) \sigma_a^{rs,k}, l_R^{rs,k}\right) + \mu_w^{rs,k} \end{cases} \tag{6}$$

The link performance function Φ is general, not limited to any specific form. We use in this paper the Bureau of Public Roads (BPR) function, as an example in Eq. (7).

$$\Phi_a(x_a) = t_{\text{ffa}}\left(1 + 0.15\left(\frac{x_a}{C_a}\right)^4\right) \tag{7}$$

The Ω function can be seen as an activation function and there are two simple forms to use: (1) linear and (2) piece-wise linear. The linear form assumes the additional travel time on through traffic caused by curb congestion is linearly dependent with curb queue length, which uses the equation $\Omega_a(v_a) = \eta_a v_a$ where η_a is the coefficient. This form indicates if there exists a curb spillover queue and even it is relatively small, it will have impact on the through traffic and cause delay. This assumption can be relaxed by using a piece-wise linear function. For cases where curb queue is smaller than a predefined threshold, the effect can be ignored and if the queue exceeds the threshold, the effect is linearly independent with queue length as shown in Eq. (8). In the numerical examples, we use linear function for simplicity.

$$\Omega_a(v_a) = \begin{cases} 0, & 0 \le v_a \le \omega \\ \eta_a v_a, & v_a \ge \omega \end{cases} \tag{8}$$

To determine link flow, there are in total q^{rs} travelers departing from r to s, and the travelers' mode choice follows a nested Logit model,

$$\begin{aligned} q_D^{rs} &= \frac{e^{-(\alpha_D + \beta\mu_D^{rs})}}{e^{-(\alpha_D + \beta\mu_D^{rs})} + e^{-(\alpha_R + \beta\mu_R^{rs})}} q^{rs} \quad \forall r \in R, s \in S \\ q_R^{rs} &= \frac{e^{-(\alpha_R + \beta\mu_R^{rs})}}{e^{-(\alpha_D + \beta\mu_D^{rs})} + e^{-(\alpha_R + \beta\mu_R^{rs})}} q^{rs} \quad \forall r \in R, s \in S \end{aligned} \tag{9}$$

Within each mode, we assume travelers follow user equilibrium (UE) to choose their respective routes, as presented in Eq. (10).

$$\begin{aligned} & f_D^{rs,k}\left(c_D^{rs,k} - \mu_D^{rs}\right) = 0 \quad \forall r \in R, s \in S \\ & f_R^{rs,k}\left(c_R^{rs,k} - \mu_R^{rs}\right) = 0 \quad \forall r \in R, s \in S \\ & c_D^{rs,k} - \mu_D^{rs} \ge 0 \\ & c_R^{rs,k} - \mu_R^{rs} \ge 0 \end{aligned} \tag{10}$$

Both the nested Logit model and UE are subject to the following constraints

$$\begin{aligned} & q_D^{rs} = \sum_{k\in K_D^{rs}} f_D^{rs,k} && \forall r \in R, s \in S \\ & q_R^{rs} = \sum_{k\in K_R^{rs}} f_R^{rs,k} && \forall r \in R, s \in S \\ & x_a = \sum_{r\in R} \sum_{s\in S} \left(\sum_{k\in K_D^{rs}} f_D^{rs,k} \delta_a^{rs,k} + \sum_{k\in K_R^{rs}} f_R^{rs,k} \sigma_a^{rs,k}\right) && \forall a \in A' \\ & f_D^{rs,k} \ge 0 && \forall k, r \in R, s \in S \\ & f_R^{rs,k} \ge 0 && \forall k, r \in R, s \in S \end{aligned} \tag{11}$$

Note that we use A' as the link set for the generalized formulation above. In the general case each curb node in the feasible vicinities of origins and destinations can break up the corresponding link into two parts. For instance, the node 4-5 in Fig. 3 splits up the link 4-5 into two links: link 4 → 4-5 and link 4-5 → 5. Then an expanded network is obtain and denoted as $G' = (N', A')$ where N' consists of both original nodes and curb nodes and A' consists of all links connecting them. Using the expanded network

we can model the flow reduction after curb nodes since some trips can end at the curb nodes. For instance, In Fig. 3, suppose there are 100 vehicles (both private driving and ride-hailing modes) entering link 4-5 from node 4 and 50 ride-hailing vehicles ends their trips at curb node 4-5. Then for link 4 → 4-5 there are 100 vehicles on it and the link travel time can be written as $\Phi_{4\to4-5}(100)+\Omega_{4\to4-5}(v^*)$ where $\Phi_{4\to4-5}$ and $\Omega_{4\to4-5}$ are link performance function and curb queue effect respectively, and v^* is the curb queue formed by the 50 ride-hailing vehicles. While for link 4-5 → 5, there are only 50 vehicles remaining and the link travel time is $\Phi_{4-5\to5}(50)+\Omega_{4-5\to5}(0)$ which has no curb queue effect. However this might be unrealistic since the curb queues do not occur at points and should have a spatial distribution across the link, making the impact to driving cost span through the whole link. To model this effect, we use an approximation that the link flow remains the same after curb node to model curb queue impact on both links broken up by curb node. Using the same example in Fig. 3, the link travel time for 4 → 4-5 now changes to $\frac{l_{4\to4-5}}{l_{4\to5}}[\Phi_{4\to5}(100)+\Omega_{4\to5}(v^*)] = 0.5\Phi_{4\to5}(100)+0.5\Omega_{4\to5}(v^*)$ and the link travel time for 4-5 → 5 changes to the $\frac{l_{4-5\to5}}{l_{4\to5}}[\Phi_{4\to5}(100)+\Omega_{4\to5}(v^*)] = 0.5\Phi_{4\to5}(100)+0.5\Omega_{4\to5}(v^*)$ where $l_{(\cdot)}$ indicates the length of link. Therefore the travel time of the entire link 4-5 is still $\Phi_{4\to5}(100)+\Omega_{4\to5}(v^*)$ and each sub-links has a fraction of the travel time with respect to the sub-link length.

In a nutshell, the general formulation is defined on an expanded network $G'=(N',A')$, whereas its approximation works on the original network (without having curb nodes splitting roadway links). In addition, they differ from the link travel time function and use different link-path relationship indicators. The approximation can be easily adopted by adding a factor to the link if the path starts or ends at the curb node at the link shown in Eq. (12). The approximation formulation is used throughout all numerical examples.

$$\begin{cases} c_D^{rs,k} = \alpha \sum_{a\in A}\left(\Phi_a(x_a)+\Omega_a(v_a)\right)\delta_a^{rs,k}\theta_{a,D}^{rs,k} + \mu_m l_D^{rs,k} + \mu_s + \mu_w^{rs,k}\tau^{rs,k} \\ c_{\mathcal{R}}^{rs,k} = \alpha \sum_{a\in A}\left[\left(\Phi_a(x_a)+\Omega_a(v_a)\right)\sigma_a^{rs,k}\theta_{a,\mathcal{R}}^{rs,k} + \gamma_a^{rs,k}w_a\right] + \Psi\left(\sum_{a\in A}\left(\Phi_a(x_a)+\Omega_a(v_a)\right)\sigma_a^{rs,k}\theta_{a,\mathcal{R}}^{rs,k}, l_{\mathcal{R}}^{rs,k}\right) + \mu_w^{rs,k} \end{cases} \tag{12}$$

where $\theta_{a,D}^{rs,k}$ is factor indicating the fraction of link a used in the path k between OD pair rs when the driving path k ends at the curb node on the link a and $\theta_{a,D}^{rs,k}$ is defined similarly for ride-hailing paths. This formulation ensures only link-path incidence matrix will be changed when using the approximation.

3.4. Equivalent variational inequality problem

The BMUE formulation can be cast into a Variational Inequality (VI) problem (Pi et al., 2019). To this end, we define a generalized cost for driving and ride-hailing, respectively

$$\begin{aligned} c_{*D}^{rs,k} &= c_D^{rs,k} + \frac{\alpha_D + \ln q_D^{rs}}{\beta} \quad \forall r\in R, s\in S \\ c_{*\mathcal{R}}^{rs,k} &= c_{\mathcal{R}}^{rs,k} + \frac{\alpha_{\mathcal{R}} + \ln q_{\mathcal{R}}^{rs}}{\beta} \quad \forall r\in R, s\in S \end{aligned} \tag{13}$$

Using the vectorized notation and consider $\mathbf{c}_*$ as a function of $\mathbf{f}=\left\{f_{\mathcal{M}}^{rs,k}\right\}$ where $\mathcal{M}\in\{D,\mathcal{R}\}$, we formulate a VI problem below, denoted by $\mathbf{VI}(\mathbf{c}_*,\Theta)$. That is to find $\mathbf{f}^*$ such that

$$\begin{aligned} &\mathbf{c}_*(\mathbf{f}^*)^\top(\mathbf{f}-\mathbf{f}^*)\geq 0 \\ &\forall \mathbf{f}\in\Theta; \\ &\Theta = \left\{\mathbf{f}=\left\{f_{\mathcal{M}}^{rs,k}\right\} \,\middle|\, \sum_{\mathcal{M}}\sum_{k\in K_{\mathcal{M}}^{rs}} f_{\mathcal{M}}^{rs,k} = q^{rs}, f_{\mathcal{M}}^{rs,k}\geq 0\right\}. \end{aligned} \tag{14}$$

Proposition 1. $\mathbf{VI}(\mathbf{c}_*,\Theta)$ *in Eq. (14) is equivalent to BMUE defined in Section 3.3.*

Proof. From the UE condition in Eqs. (9) and (10), we have

$$\begin{aligned} \mu_{\mathcal{M}}^{rs} &= -\frac{1}{\beta}\left[\alpha_{\mathcal{M}} + \ln q_{\mathcal{M}}^{rs} + \ln\frac{\sum_{\mathcal{M}} e^{-(\alpha_{\mathcal{M}}+\beta\mu_{\mathcal{M}}^{rs})}}{q^{rs}}\right] \\ c_{\mathcal{M}}^{rs,k} - \mu_{\mathcal{M}}^{rs} &= c_{\mathcal{M}}^{rs,k} + \frac{\alpha_{\mathcal{M}}+\ln q_{\mathcal{M}}^{rs}}{\beta} + \mathscr{C}(rs) \end{aligned} \tag{15}$$

where $\mathscr{C} = \frac{1}{\beta}\ln\frac{\sum_{\mathcal{M}} e^{-(\alpha_{\mathcal{M}}+\beta\mu_{\mathcal{M}}^{rs})}}{q^{rs}}$, which is same for all paths of both modes between each OD pair solely depending on rs. Now suppose

$$\begin{aligned} &\mathbf{c}_* = \{c_{*\mathcal{M}}^{rs,k}\}, \quad c_{*\mathcal{M}}^{rs,k} = c_{\mathcal{M}}^{rs,k} + \frac{\alpha_{\mathcal{M}}+\ln q_{\mathcal{M}}^{rs}}{\beta} \\ &\tilde{\mathbf{c}}_* = \{\tilde{c}_{*\mathcal{M}}^{rs,k}\}, \quad \tilde{c}_{*\mathcal{M}}^{rs,k} = c_{\mathcal{M}}^{rs,k} + \frac{\alpha_{\mathcal{M}}+\ln q_{\mathcal{M}}^{rs}}{\beta} + \mathscr{C}(rs) \end{aligned} \tag{16}$$

then $\forall \mathbf{f} \in \Theta$ we have,

$$\mathbf{c}_*(\mathbf{f}^*)^\top(\mathbf{f}-\mathbf{f}^*) = (\mathbf{c}_*(\mathbf{f}^*)+\mathscr{C})^\top(\mathbf{f}-\mathbf{f}^*) = \tilde{\mathbf{c}}_*(\mathbf{f}^*)^\top(\mathbf{f}-\mathbf{f}^*) \tag{17}$$

Thus, $\mathbf{VI}(\mathbf{c}_*, \Theta)$ is equivalent to $\mathbf{VI}(\tilde{\mathbf{c}}_*, \Theta)$.

Based on the proposition in Nagurney (2009) and Pi et al. (2019), let $\tilde{\mathbf{c}}_* : \mathbb{R}^n \mapsto \mathbb{R}^n$ and Θ be a non-negative orthant of $\mathbf{f}^* \in \mathbb{R}^n$, then we have $\mathbf{VI}(\tilde{\mathbf{c}}_*, \Theta)$ has same solutions as the following complementary problem:

$$\text{Find } \mathbf{f}^* \geq 0 \text{ such that } \tilde{\mathbf{c}}_*(\mathbf{f}^*) \geq 0 \text{ and } \tilde{\mathbf{c}}_*(\mathbf{f}^*)^\top \mathbf{f}^* = 0 \tag{18}$$

Based on the BMUE condition, we know $\tilde{\mathbf{c}}_*(\mathbf{f}^*)^\top \mathbf{f}^* = 0$ and $\tilde{\mathbf{c}}_*(\mathbf{f}^*) \geq 0$. Therefore, $\mathbf{VI}(\tilde{\mathbf{c}}_*, \Theta)$ solves for the network flow under BMUE. As a result, $\mathbf{VI}(\mathbf{c}_*, \Theta)$ is equivalent to BMUE. □

3.5. Solution algorithm for BMUE

The VI formulation defined above can be efficiently solved using heuristics, projection-based method, or feasible direction algorithm. One widely used heuristics algorithm is the method of successive averages (MSA) (Sheffi, 1985). In this paper we use MSA with a heuristic column generation approach to solve the VI problem. Detailed discussions on convergence and effectiveness of the MSA algorithm can be found in Ma and Qian (2017) and Pi et al. (2019).

Since this is an iterative algorithm, we adopt an adjustable step size Δ_f, which will be chosen differently for different networks. The initial path set is generated by a shortest path algorithm and the size is predefined to be small, i.e. 3 paths for each modes. In each iteration of MSA, after performing network loading with current path flow, new shortest paths, if different from paths in the current path set, will be identified and added in the current path set until no more shorter paths can be found or the path set size reaches the predefined upper-bound limit ξ.

Algorithm 1: MSA with a heuristic path column generation method

Initialize all path flow $\mathbf{f}$ in the initial path set to $\mathbf{0}$;
Compute cost for all initial paths $\mathbf{c}$ with the empty network;
for $(r,s) \in R \times S$ **do**
  Identify path $k^* \in K_D^{rs} \cup K_R^{rs}$ with the lowest path cost;
  Set $f_{\mathcal{M}}^{rs,k^*} = q^{rs}$;
end
Set iteration $i = 1$;
repeat
  Perform network loading with current path flow $\mathbf{f}$;
  for $(r,s) \in R \times S$ **do**
    Perform shortest path algorithm to identify the path with smallest generalized cost, denoted as k^*;
    if $k^* \in K_D^{rs} \cup K_R^{rs}$ ***or*** $|K_D^{rs} \cup K_R^{rs}| = \xi$ **then**
      Maintain current path set $K_D^{rs} \cup K_R^{rs}$
    end
    if $k^* \notin K_D^{rs} \cup K_R^{rs}$ ***and*** $|K_D^{rs} \cup K_R^{rs}| < \xi$ **then**
      Append k^* to path set $K_D^{rs} \cup K_R^{rs}$ accordingly
    end
    Set $f_{\mathcal{M}}^{rs,k^*} = f_{\mathcal{M}}^{rs,k^*} + \sum_{k \in K_D^{rs} \cup K_R^{rs}, k \neq k^*} \frac{\Delta_f}{i} f_{\mathcal{M}}^{rs,k}$;
    For all $k \in K_D^{rs} \cup K_R^{rs}$, $k \neq k^*$, set $f_{\mathcal{M}}^{rs,k} = \left(1 - \frac{\Delta_f}{i}\right) f_{\mathcal{M}}^{rs,k}$;
  end
  Set $i = i + 1$;
until *The network flow converges*;

4. Optimal curb pricing (OCP) design

4.1. Formulation

Based on the proposed BMUE model presented in Sections 3.3 and 3.4, a framework is developed to determine the optimal curb prices for ride-hailing stops (PUDOs) in order to achieve system optimum (SO) for the entire transportation network. The curbside pricing may be one possible economic instrument to influence demand behavior of PUDO to improve system performance. Curbside pricing means that if a ride-hailing vehicle makes a stop to PUDO passengers at link a, then the traveler would need to pay μ_a for the use of curbside space and the corresponding path cost for this traveler would increase by μ_a. The intuition is to regulate the curbside queue distribution throughout the network by imposing curbside charges, which in turn would further change the travelers'

choices in modes and routes, redirecting user equilibrium patterns. To this end, an additional curbside use fee $\mu_a \geq 0$ is introduced for each link $a \in A'$. Therefore, the cost function Eq. (6) for both modes can be rewritten as,

$$\begin{aligned} c_D^{rs,k} &= \alpha \sum_{a \in A'} \left(\Phi_a(x_a) + \Omega_a(v_a)\right) \delta_a^{rs,k} + \mu_m l_D^{rs,k} + \mu_s + \mu_w^{rs,k} \tau^{rs,k} \\ c_{\mathcal{R}}^{rs,k} &= \alpha \sum_{a \in A'} \left[\left(\Phi_a(x_a) + \Omega_a(v_a)\right) \sigma_a^{rs,k} + \gamma_a^{rs,k} w_a\right] + \Psi\left(\sum_{a \in A'} \left(\Phi_a(x_a) + \Omega_a(v_a)\right) \sigma_a^{rs,k}, l_{\mathcal{R}}^{rs,k}\right) + \mu_w^{rs,k} + \sum_{a \in A'} \gamma_a^{rs,k} \mu_a \end{aligned} \tag{19}$$

where $\gamma_a^{rs,k}$ is the indicator variable as stated in Eq. (1). Also Eq. (12) can be used by adding a curb charge when the origin link set A is used with the approximation of link travel cost. To achieve system optimum, we define the objective function in Eq. (20), which is the total social cost across two modes. The curbside charge collected by the public agencies can be re-distributed to the general public through infrastructure improvement or public services, and then is considered as part of the social welfare, not included in the total social cost. The constraints are the VI formulation for solving network flow under BMUE, with additional upper and lower bound for the curbside charge for each link.

$$\begin{aligned} &\min_{\{\mu_a\}} \sum_{r \in R} \sum_{s \in S} \left[\sum_{k \in K_D^{rs}} f_{\text{penalty}}\left(f_D^{rs,k} \cdot c_D^{rs,k}\right) + \sum_{k \in K_{\mathcal{R}}^{rs}} f_{\text{penalty}}\left(f_{\mathcal{R}}^{rs,k} \cdot \left(c_{\mathcal{R}}^{rs,k} - \sum_{a \in A'} \gamma_a^{rs,k} \mu_a\right)\right)\right] \\ &\text{s.t.} \quad \mathbf{c}_*(\mathbf{f}^*)^\top (\mathbf{f} - \mathbf{f}^*) \geq 0 \\ &\quad \forall \mathbf{f} \in \Theta = \left\{ \left\{ f_D^{rs,k}, f_{\mathcal{R}}^{rs,k} \right\} \Big| \sum_{k \in K_D^{rs}} f_D^{rs,k} + \sum_{k \in K_{\mathcal{R}}^{rs}} f_D^{rs,k} = q^{rs}, f_D^{rs,k} \geq 0, f_{\mathcal{R}}^{rs,k} \geq 0, \forall rs \right\}. \\ &\quad \mu_a^- \leq \mu_a \leq \mu_a^+, \forall a \end{aligned} \tag{20}$$

where $f_{\text{penalty}}(\cdot)$ is penalty function.

Remark 3. In this paper, $f_{\text{penalty}}(x)$ indicates a generalized penalty function. In our numerical examples, $f_{\text{penalty}}(x) = x$ is chosen so that the objective function in Eq. (20) represents the total generalized travel cost of all travelers. The options of using quadratic, exponential penalty function could also be considered to penalize more heavily on any potentially extreme value of path cost on a used path.

Remark 4. In a more general setting, μ_a^- and μ_a^+ are lower and upper bound for the curb parking price for link a. If we set $\mu_a^- = 0$ and $\mu_a^+ > 0$, it means only curb parking fee is considered and if we set $\mu_a^- < 0$ and $\mu_a^+ > 0$, it means there can be incentives for ride-hailing vehicles attracting ride-hailing vehicles to park at desired curbs. In our numerical experiments, we only consider curb parking fee and no incentive is given to ride-hailing travelers.

Remark 5. Eq. (20) can be seen as a bi-level optimization problem. The upper level is to minimize the total social cost and the lower level is user equilibrium for two modes where travelers choose both modes and routes. Hence sensitivity analysis-based solution algorithms can be used to solve the OCP problem.

4.2. Vectorization

We vectorize all the variables in the BMUE model before presenting a solution algorithm. We denote function $\mathbf{\Phi}(\mathbf{x})$ and $\mathbf{\Omega}(\mathbf{q})$ as the vectorized functions over all links. For all of the vectors defined, there are three different sets of indices: $a \in A'$; $r \in R, s \in S, k \in K_{\mathcal{M}}^{rs}$; and $r \in R, s \in S$. For each set of indices, we fix an order of indexing and use the indexing throughout the model. Matrices mentioned in notation list should also follow the same indexing order here. The vectorized form of Eq. (20) can be reformulated as

$$\begin{aligned} &\min_{\mathbf{m}} \mathbf{f} \cdot \mathbf{c}' \\ &s.t. \quad \mathbf{c}_*(\mathbf{f}^*)^\top (\mathbf{f} - \mathbf{f}^*) \geq 0 \\ &\quad \forall \mathbf{f} \in \Theta = \left\{ \mathbf{f} \middle| \Lambda \mathbf{f} = \mathbf{q}, \mathbf{f} \geq 0 \right\}. \\ &\quad \mathbf{m}^- \leq \mathbf{m} \leq \mathbf{m}^+ \end{aligned} \tag{21}$$

where $\mathbf{c}'$ differs from $\mathbf{c}$ by the curb charge for each ride-hailing path.

4.3. Sensitivity analysis-based solution algorithm

Since the constraints of the optimization problem are BMUE, the problem is non-convex and it is generally difficult to solve. In this section, we develop a sensitivity analysis-based approach to approximate the gradient of the objective function with respect to the curbside prices $\mathbf{m}$, due to the fact that directly computing the derivative of the objective function is challenging (Tobin and Friesz, 1988; Yang, 1997). Then the projected gradient descent algorithm can be applied to minimize the system costs and determine the optimal curb prices.

Let Λ and Δ denote the O–D/path and link/path incidence matrices associated with the equilibrated path. $\mathbf{f}, \mathbf{q}, \mathbf{c}$ are the vector tabulations for path flow, O-D pair demands and path costs, respectively. From the BMUE we have,

$$\begin{bmatrix} \Delta \\ \Lambda \end{bmatrix} \mathbf{f} = \begin{bmatrix} \mathbf{x} \\ \mathbf{q} \end{bmatrix} \tag{22}$$

Search all the linear independent paths in set of $\mathbf{f}$ to obtain a non-degenerate path set $\tilde{\mathbf{f}}$ and the corresponding $\tilde{\Delta}$ and $\tilde{\Lambda}$, then we have

$$\begin{bmatrix} \tilde{\Delta} \\ \tilde{\Lambda} \end{bmatrix} \tilde{\mathbf{f}} = \begin{bmatrix} \mathbf{x} \\ \mathbf{q} \end{bmatrix} \tag{23}$$

Remark 6. There are many options to obtain a linear independent path set $\tilde{\mathbf{f}}$ in Eq. (23). In this paper, we solve the linear programming (LP) problem (24) to obtain $\tilde{\mathbf{f}}$ (Tobin and Friesz, 1988). The weight $\mathbf{w}$ in objective function can be any positive value vector. $\tilde{\mathbf{f}}$ contains only all positive elements from the solution of the LP problem, such that $|\tilde{\mathbf{f}}| = rank\left(\begin{bmatrix} \Delta \\ \Lambda \end{bmatrix}\right)$.

$$\begin{aligned} &\tilde{\mathbf{f}} = \arg\min_{\hat{\mathbf{f}}} \mathbf{w}^{\top}\hat{\mathbf{f}} \\ &\text{s.t.} \begin{bmatrix} \Delta \\ \Lambda \end{bmatrix} \hat{\mathbf{f}} = \begin{bmatrix} \mathbf{x} \\ \mathbf{q} \end{bmatrix} \\ &\hat{\mathbf{f}} \geq 0 \end{aligned} \tag{24}$$

Further denote $\boldsymbol{\pi}$ as a vector representing the minimum cost between all O-D pairs and $\tilde{\mathbf{c}}$ the path cost for the new path set $\tilde{\mathbf{f}}$. Based on the optimality condition of BMUE and O-D demand conservation, we have,

$$\begin{aligned} \tilde{\mathbf{c}}(\tilde{\mathbf{f}}, \mathbf{m}) - \tilde{\Lambda}^{\top}\boldsymbol{\pi} = 0 \\ \tilde{\Lambda}\tilde{\mathbf{f}} - \mathbf{q} = 0 \end{aligned} \tag{25}$$

Taking the derivative with respect to $\mathbf{m}$, we obtain

$$\begin{bmatrix} \nabla_{\tilde{\mathbf{f}}}\tilde{\mathbf{c}}(\tilde{\mathbf{f}}, \mathbf{m}) & -\tilde{\Lambda}^{\top} \\ \tilde{\Lambda} & 0 \end{bmatrix} \begin{bmatrix} \nabla_{\mathbf{m}}\tilde{\mathbf{f}} \\ \nabla_{\mathbf{m}}\boldsymbol{\pi} \end{bmatrix} = \begin{bmatrix} -\nabla_{\mathbf{m}}\tilde{\mathbf{c}}(\tilde{\mathbf{f}}, \mathbf{m}) \\ 0 \end{bmatrix} \tag{26}$$

Let

$$J_{\tilde{\mathbf{f}},\mathbf{m}} = \begin{bmatrix} \nabla_{\tilde{\mathbf{f}}}\tilde{\mathbf{c}}(\tilde{\mathbf{f}}, \mathbf{m}) & -\tilde{\Lambda}^{\top} \\ \tilde{\Lambda} & 0 \end{bmatrix} \tag{27}$$

and it can be shown the Jacobian $J_{\tilde{\mathbf{f}},\mathbf{m}}$ is nonsingular. Denote the inverse of Jacobian matrix as

$$J_{\tilde{\mathbf{f}},\mathbf{m}}{}^{-1} = \begin{bmatrix} B_{11} & B_{12} \\ B_{21} & B_{22} \end{bmatrix} \tag{28}$$

with matched sub-dimensions and sub-dimension matrices are as follows:

$$\begin{aligned} B_{22} &= \left[\tilde{\Lambda}\nabla_{\tilde{\mathbf{f}}}\tilde{\mathbf{c}}(\tilde{\mathbf{f}}, \mathbf{m})^{-1}\tilde{\Lambda}^{\top}\right]^{-1} \\ B_{21} &= -\left[\tilde{\Lambda}\nabla_{\tilde{\mathbf{f}}}\tilde{\mathbf{c}}(\tilde{\mathbf{f}}, \mathbf{m})^{-1}\tilde{\Lambda}^{\top}\right]^{-1}\tilde{\Lambda}\nabla_{\tilde{\mathbf{f}}}\tilde{\mathbf{c}}(\tilde{\mathbf{f}}, \mathbf{m})^{-1} \\ B_{12} &= \nabla_{\tilde{\mathbf{f}}}\tilde{\mathbf{c}}(\tilde{\mathbf{f}}, \mathbf{m})^{-1}\tilde{\Lambda}^{\top}\left[\tilde{\Lambda}\nabla_{\tilde{\mathbf{f}}}\tilde{\mathbf{c}}(\tilde{\mathbf{f}}, \mathbf{m})^{-1}\tilde{\Lambda}^{\top}\right]^{-1} \\ B_{11} &= \nabla_{\tilde{\mathbf{f}}}\tilde{\mathbf{c}}(\tilde{\mathbf{f}}, \mathbf{m})^{-1}\left[I - \tilde{\Lambda}^{\top}\left(\tilde{\Lambda}\nabla_{\tilde{\mathbf{f}}}\tilde{\mathbf{c}}(\tilde{\mathbf{f}}, \mathbf{m})^{-1}\tilde{\Lambda}^{\top}\right)^{-1} \cdot \tilde{\Lambda}\nabla_{\tilde{\mathbf{f}}}\tilde{\mathbf{c}}(\tilde{\mathbf{f}}, \mathbf{m})^{-1}\right] \end{aligned} \tag{29}$$

Then, we can rewrite Eq. (26) as

$$\begin{bmatrix} \nabla_{\mathbf{m}}\tilde{\mathbf{f}} \\ \nabla_{\mathbf{m}}\boldsymbol{\pi} \end{bmatrix} = \begin{bmatrix} B_{11} & B_{12} \\ B_{21} & B_{22} \end{bmatrix} \begin{bmatrix} -\nabla_{\mathbf{m}}\tilde{\mathbf{c}}(\tilde{\mathbf{f}}, \mathbf{m}) \\ 0 \end{bmatrix} \tag{30}$$

In particular, we have

$$\nabla_{\mathbf{m}}\tilde{\mathbf{f}} = -B_{11}\nabla_{\mathbf{m}}\tilde{\mathbf{c}}(\tilde{\mathbf{f}}, \mathbf{m}) \tag{31}$$

and

$$\begin{aligned} \nabla_{\mathbf{m}}\mathbf{f} &= \nabla_{\mathbf{m}}\Delta^{\top}\mathbf{x} \\ &= \Delta^{\top}\nabla_{\mathbf{m}}\mathbf{x} \\ &= \Delta^{\top}\tilde{\Delta}\nabla_{\mathbf{m}}\tilde{\mathbf{f}} \\ &= -\Delta^{\top}\tilde{\Delta}B_{11}\nabla_{\mathbf{m}}\tilde{\mathbf{c}}(\tilde{\mathbf{f}}, \mathbf{m}) \end{aligned} \tag{32}$$

Therefore, we have the gradient of total social cost with respect to curb price $\mathbf{m}$,

$$\begin{aligned} \nabla_{\mathbf{m}}(\mathbf{f} \cdot \mathbf{c}') &= \left(\nabla_{\mathbf{m}}\mathbf{f}\right)^{\top}\mathbf{c}' + \mathbf{f}^{\top}\nabla_{\mathbf{m}}\mathbf{c}' \\ &= \left(\nabla_{\mathbf{m}}\mathbf{f}\right)^{\top}\mathbf{c}' \\ &= -\left[\Delta^{\top}\tilde{\Delta}B_{11}\nabla_{\mathbf{m}}\tilde{\mathbf{c}}(\tilde{\mathbf{f}}, \mathbf{m})\right]^{\top}\mathbf{c}' \end{aligned} \tag{33}$$

Given that $\mathbf{c}'$ is free of $\mathbf{m}$ and thus $\nabla_{\mathbf{m}}\mathbf{c}' = 0$. This derivative can be computed with $\nabla_{\mathbf{f}}\mathbf{c}$ and $\nabla_{\mathbf{m}}\mathbf{c}$, which can be expressed explicitly and relatively easy to obtain. To compute the derivatives of $\mathbf{c}$, we assume a linear ride-hailing price function presented in Eq. (34), which is similar to the charge mechanism of Uber. The ride-hailing service price linearly depends on travel time and travel distance with different coefficients, and includes a baseline service fee term,

$$\Psi(t, l) = \alpha_\Psi t + \beta_\Psi l + \gamma_\Psi \tag{34}$$

We rewrite the cost function in the following vector form,

$$\mathbf{c} = \mathbf{C}_1 \Delta^\intercal(\mathbf{\Phi} + \mathbf{\Omega}) + \mathbf{\Gamma}^\intercal \mathbf{m} + \mathbf{C}_2 \mathbf{\Gamma}^\intercal \mathbf{w} \tag{35}$$

where $\mathbf{C}_1$ and $\mathbf{C}_2$ are constant diagonal matrices representing the coefficients of value of time and can be computed easily. $\mathbf{\Gamma}$ is $0-1$ indicator matrix mapping each path to the links it starts from and ends at ($\gamma_a^{rs,k}$ in vectorized form), thus we have $\mathbf{p} = \mathbf{\Gamma}\mathbf{f}$. Then, we can compute the derivatives $\nabla_{\mathbf{m}}\mathbf{c}$ and get the final gradient in Eq. (33).

$$\begin{aligned}
\nabla_{\mathbf{m}}\mathbf{c} &= \mathbf{\Gamma}^\intercal \\
\nabla_{\mathbf{f}}\mathbf{c} &= \mathbf{C}_1 \Delta^\intercal \left(\nabla_{\mathbf{x}}\mathbf{\Phi} \cdot \nabla_{\mathbf{f}}\mathbf{x} + \nabla_{\mathbf{v}}\mathbf{\Omega} \cdot \nabla_{\lambda_1}\mathbf{v} \cdot \nabla_{\mathbf{p}}\lambda_1 \cdot \nabla_{\mathbf{f}}\mathbf{p} \right) + \mathbf{C}_2 \mathbf{\Gamma}^\intercal \cdot \nabla_{\lambda_1}\mathbf{w} \cdot \nabla_{\mathbf{p}}\lambda_1 \cdot \nabla_{\mathbf{f}}\mathbf{p} \\
&= \mathbf{C}_1 \Delta^\intercal \left(\nabla_{\mathbf{x}}\mathbf{\Phi} \cdot \Delta + \nabla_{\mathbf{v}}\mathbf{\Omega} \cdot \nabla_{\lambda_1}\mathbf{v} \cdot \nabla_{\mathbf{p}}\lambda_1 \cdot \mathbf{\Gamma} \right) + \mathbf{C}_2 \mathbf{\Gamma}^\intercal \cdot \nabla_{\lambda_1}\mathbf{w} \cdot \nabla_{\mathbf{p}}\lambda_1 \cdot \mathbf{\Gamma}
\end{aligned} \tag{36}$$

Note that here $\nabla_{\mathbf{x}}\mathbf{\Phi}, \nabla_{\mathbf{v}}\mathbf{\Omega}, \nabla_{\lambda_1}\mathbf{v}, \nabla_{\lambda_1}\mathbf{w}, \nabla_{\mathbf{p}}\lambda_1$ are diagonal matrices with each diagonal entry $\frac{d\Phi_a}{dx_a}$, $\frac{d\Omega_a}{dv_a}$, $\frac{dv_a}{d\lambda_{a,1}}$, $\frac{dw_a}{d\lambda_{a,1}}$, $\frac{d\lambda_{1a}}{dp_a}$ where

$$\begin{aligned}
\frac{d\Phi_a}{dx_a} &= 0.6 t_{\mathrm{ff}a} \left(\frac{x_a^3}{C_a^4} \right) \\
\frac{dv_a}{d\lambda_{a,1}} &= \begin{cases} \frac{\lambda_{a,2}}{(\lambda_{a,2}-\lambda_{a,1})^2} & \lambda_{a,2} - \lambda_{a,1} \geq \epsilon \\ \epsilon^{-1} & \lambda_{a,2} - \lambda_{a,1} < \epsilon \end{cases} \\
\frac{dw_a}{d\lambda_{a,1}} &= \frac{1}{(\lambda_{a,2} - \lambda_{a,1})^2} \mathbf{1}(\lambda_{a,2} - \lambda_{a,1} \geq \epsilon) \\
\frac{d\lambda_{1a}}{dp_a} &= t_t^{-1}
\end{aligned} \tag{37}$$

Finally, Eq. (36) shows the Jacobian matrix with respect to full path set $\mathbf{f}$ and we can choose corresponding rows and columns of the Jacobian matrix to obtain $\nabla_{\mathbf{m}}\tilde{\mathbf{c}}(\tilde{\mathbf{f}}, \mathbf{m})$ and $\nabla_{\tilde{\mathbf{f}}}\tilde{\mathbf{c}}(\tilde{\mathbf{f}}, \mathbf{m})$. Then the gradient of interest, $\nabla_{\mathbf{m}}(\mathbf{f} \cdot \mathbf{c}')$ can be obtained using Eq. (33) and projected gradient descent algorithm can be performed to solve the optimization problem. Since this is also an iterative solver, the choice of step size in each iteration is crucial. There are many options to choose the step size. Either fixed or adaptive step size can be used in practice. In this study, we use a decaying step size with iterations. We also normalize the gradient before computing update to make gradient-based algorithm less sensitive to some extreme large or small partial gradients.

Algorithm 2: Projected Gradient Descent for Optimal Curb Pricing

Initialize curb charges at all links $\mathbf{m}$ to a preset value (a constant vector);
Set counter $i = 1$ (the number of iterations);
repeat
  Use **Algorithm** 1 to solve for BMUE;
  Compute the gradient $\nabla_{\mathbf{m}}(f \cdot c')$ as derived in Equation (33) and (36) accordingly;
  Update the curb price using normalised gradient and perform projection to the constrained set

$$\mathbf{m} = \Pi_D \left(\mathbf{m} - \frac{\eta}{\sqrt{i}} \bar{\nabla}_{\mathbf{m}}(f \cdot c') \right) = \arg\min_{\mathbf{z} \in D} \|\mathbf{z} - \mathbf{m}\|_2^2 \tag{38}$$

  where $\bar{\nabla}_{\mathbf{m}}(f \cdot c') = \nabla_{\mathbf{m}}(f \cdot c') / \left[\max(\nabla_{\mathbf{m}}(f \cdot c')) - \min(\nabla_{\mathbf{m}}(f \cdot c')) \right]$, $D = \{\mathbf{m} | \mathbf{m}_l \leq \mathbf{m} \leq \mathbf{m}_u\}$;
  Set $i = i + 1$;
until *The curb prices* $\mathbf{m}$ *converge*;

5. Numerical experiments

In this section, we examine the proposed BMUE model and the sensitivity-based solution algorithm for solving optimal curb pricing on three networks: a 6-link toy network, Sioux-Falls network and Pittsburgh Downtown network.

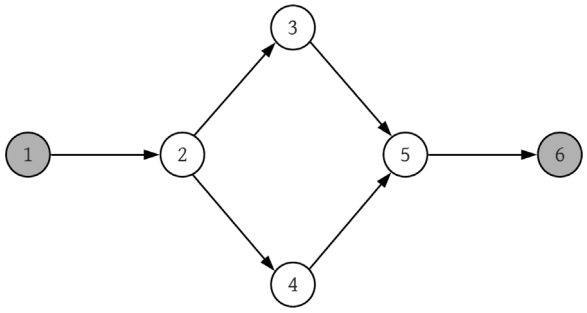

Fig. 4. The 6-link network.

Table 2
The 6-link network link properties.

Link id	Flow capacity C_a (veh/T)	Length l_a (mile)	Free flow time t_{ffa} (min)	Curb location
$1 \to 2$	2000	0.8	1.2	0.2
$2 \to 3$	3500	2.0	3.0	0.5
$2 \to 4$	2000	1.5	3.0	0.5
$3 \to 5$	3500	1.6	2.4	0.5
$4 \to 5$	2000	1.5	3.0	0.5
$5 \to 6$	2000	1.0	1.5	0.8

Table 3
Network parameters and model coefficients for 6-link network.

Name	Value
Total commute duration T	90 min
Unit time cost α	0.7 \$/min
The per mile unit cost constant for driving μ_m	1.5 \$/mile
Average time for vehicles to complete curbside stops t_c	2 min
Constant for logit choice model α_D	1
Constant for logit choice model α_R	2
Constant for logit choice model β	1
Constant to regulate queuing model ϵ	0.01
Maximum walking distance before pick-ups or after drop-offs ζ	1 mile
Default curb capacity κ (assumed to be identical for all links)	50 veh/mile

5.1. 6-link toy network

We start from a 6-link toy network to validate the effectiveness and robustness of proposed models. An overview of the 6-link network is presented in Fig. 4. In the network, the node and link set are indicated as $V = \{1, 2, 3, 4, 5, 6\}$ and $A = \{1 \to 2, 2 \to 3, 2 \to 4, 3 \to 5, 4 \to 5, 5 \to 6\}$ respectively. The origin and destination sets both contain one node which are $R = \{1\}$ and $S = \{6\}$ respectively, with the O-D demand of q^{16}. For each link, the associated properties are listed in Table 2. Note here the curb location indicates where each curb node locates relatively on the link to the starting node. For instance, the curb node 1-2 on link $1 \to 2$ has a distance of $0.8 \times 0.2 = 0.16$ from starting node 1. Other default network parameters and model coefficients are shown in Table 3.

Similar to the fare structure of Uber, we choose the ride-hailing fare function $\Psi(t, l) = 0.35t + 1.75l + 2.55$. Due to the lack of data to calibrate the activation function $\mathbf{\Omega}$ for the effect of curbside stops to through traffic on driving lanes, we assume a simple linear function to model this effect $\mathbf{\Omega}_a = 0.05v_a$. Note that the ride-hailing fare Ψ and activation function $\mathbf{\Omega}$ remain the same throughout all the numerical experiments.

A fixed cost μ_s is assumed as the parking fee for any drivers heading to destination $s \in S$. This approximates the anticipated parking cost all parking options near a destination, which allows us to explore the effect of curbside pricing with a simplified parking fee structure. To compute walking cost $\mu_w^{rs,k}$ for ride-hailing users and driving users choosing parking off-street/on-street for $r \in R, s \in S, k \in K_R^{rs}$ or K_D^{rs}, we use the walking distance $l_w^{rs,k}$ divided by average walking speed which is assumed as 0.05 miles per min.

$$\mu_w^{rs,k} := \frac{\alpha l_w^{rs,k}}{0.05}$$

For the 6-link network, we choose the maximum radius to compute vicinity of a node ζ to be 1 mile and assume all curb nodes are allowed for ride-hailing stops and private vehicles accessibility to parking. Then the feasible vicinity of the origin node 1 and destination node 6 are {1-2} and {5-6} respectively. Since the path set is small, we use the full path set as the initial path set and

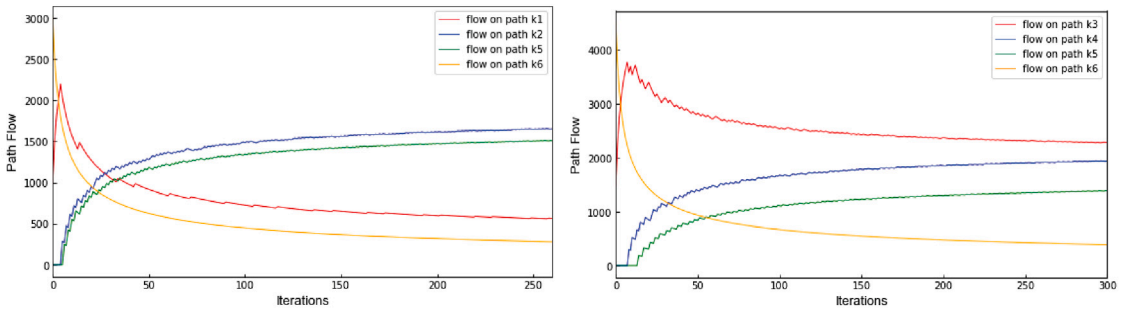

(a) Scenario: $q^{16} = 4000$ (b) Scenario: $q^{16} = 6000$

Fig. 5. Convergence of flow on different paths.

column generation is not needed in each iteration of BMUE solver. Therefore we can generate four driving paths considering parking location choice

$$\begin{aligned} k_1 &: 1 \to 2 \to 3 \to 5 \to 6 \\ k_2 &: 1 \to 2 \to 4 \to 5 \to 6 \\ k_3 &: 1 \to 2 \to 3 \to 5 \to 5\text{-}6 \\ k_4 &: 1 \to 2 \to 4 \to 5 \to 5\text{-}6 \end{aligned}$$

and two ride-hailing paths considering PUDO location choice

$$\begin{aligned} k_5 &: 1\text{-}2 \to 2 \to 3 \to 5 \to 5\text{-}6 \\ k_6 &: 1\text{-}2 \to 2 \to 4 \to 5 \to 5\text{-}6 \end{aligned}$$

In this and following examples we use the original link set A to handle the link travel time and the approximation stated in Section 3.3 is used meaning the flow reduction is not considered and the curb queue impact is even distributed throughout the link.

5.1.1. BMUE solution

First, we run BMUE with the O-D demand $q^{16} = 4000$ (veh/T) without curb pricing. The resulting path flows and the corresponding path costs at equilibrium are,

$$\begin{aligned} &f_D^{16,k_1} = 564.4, f_D^{16,k_2} = 1650.4, f_D^{16,k_3} = 0.0, f_D^{16,k_4} = 0.0, f_R^{16,k_5} = 1506.5, f_R^{16,k_6} = 278.7. \\ &c_D^{16,k_1} = 43.99, c_D^{16,k_2} = 43.98, c_D^{16,k_3} = 45.78, c_D^{16,k_4} = 45.77, c_R^{16,k_5} = 43.97, c_R^{16,k_6} = 44.26. \end{aligned} \tag{39}$$

Then we run BMUE with $q^{16} = 6000$ for comparison and the results are as follows,

$$\begin{aligned} &f_D^{16,k_1} = 0.0, f_D^{16,k_2} = 0.0, f_D^{16,k_3} = 2281.4, f_D^{16,k_4} = 1944.8, f_R^{16,k_5} = 1389.4, f_R^{16,k_6} = 384.4. \\ &c_D^{16,k_1} = 60.30, c_D^{16,k_2} = 60.30, c_D^{16,k_3} = 59.95, c_D^{16,k_4} = 59.95, c_R^{16,k_5} = 59.95, c_R^{16,k_6} = 60.26. \end{aligned} \tag{40}$$

The convergence of path flows for these two scenarios is shown in Fig. 5.

The results indicate that when demand is 4000, driving paths k_3 and k_4 for the driving mode are not chosen by travelers since parking at curbside and then walking to destination will generate larger path cost. But when demand increases to 6000, driving paths k_1 and k_2 are not chosen because link $5 \to 6$ is too congested due to a queue induced by curbside stops, then travelers prefer to park near the curbside and than walk to the destination.

In addition, we solve BMUE in other settings by varying driving parking cost and curb space capacity. The results are summarized in Table 4. We can see that path flows at equilibrium are sensitive to not only the total demand, but also to curbside configurations (i.e. capacity) and parking cost for driving mode. With the increase in demand, more travelers prefer driving because as the network becomes congested, the cost of ride-hailing will be larger than driving due to a greater time-related service fare. When O-D demand is between 2000 and 5000, no traveler chooses to parking near the curb, but when O-D demand reaches high 6000, all driving travelers choose parking near the curb. This can be interpreted as link 5-6 is more congested and driving takes more time to traverse that link, so it is more convenient to park near the curb than park at the destination. The result also demonstrates that increasing parking fee for driving will attract more travelers to choose ride-hailing, but the effectiveness of that shift for each unit increase in parking fee levels off once the parking fee increases up to a threshold (i.e. 50 in this case). The mode choice is also sensitive to the curbside capacity. A greater curbside capacity indicates the curb can accommodate more PUDOs with less curb-induced queues, making ride-hailing more favorable. The curbside capacity is the most effective in impacting mode choices when it increases from small to medium, but not so much when the space is already plenty. Overall, from a policy making perspective, when curb space for ride-hailing stops is very limited (as a result of either full on-street parking or very limited designated spaces for ride-hailing stops), increasing curb capacity effectively reduces curb waiting time and thus encourages commuters to use ride-hailing services favorably over driving.

Table 4
BMUE solutions in different settings.

Demand (veh/90 min)	Parking cost ($)	Curb capacity (veh/mile)	f_D^{16,k_1}	f_D^{16,k_2}	f_D^{16,k_3}	f_D^{16,k_4}	f_D^{16,k_5}	f_D^{16,k_6}
2000	20	50	16.8	199.4	0.0	0.0	350.0	1,433.8
3000	20	50	234.3	982.7	0.0	0.0	1,106.7	676.2
4000	20	50	564.4	1,650.4	0.0	0.0	1,506.5	278.7
5000	20	50	1,517.3	1,700.7	0.0	0.0	1,392.9	389.1
6000	20	50	0.0	0.0	2,281.4	1,944.8	1,389.4	384.4
7000	20	50	0.0	0.0	4,302.1	2,447.1	74.2	176.6
4000	10	50	2,148.3	1,804.1	0.0	0.0	47.6	0.0
4000	50	50	185.6	1,572.4	0.0	0.0	2,058.9	183.1
4000	100	50	166.7	1,587.2	0.0	0.0	2,081.5	164.6
4000	20	25	1,464.6	1,460.3	0.0	0.0	734.2	340.9
4000	20	75	76.6	780.6	0.0	0.0	2,288.9	853.9
4000	20	100	47.6	407.6	0.0	0.0	2,318.0	1,226.8
4000	20	200	33.6	342.2	0.0	0.0	2,330.4	1,293.8

Table 5
Optimal curbside price in different settings.

Demand (veh/90 min)	Parking fee ($)	Curb capacity (veh/mile)	OCP ($)	Total social cost ($)		
				w/o pricing	w/ OCP (reduction)	SO (reduction)
2000	20	50	1.24	70,054.33	62,514.15 (−10.8%)	54,401.23 (−22.3%)
3000	20	50	2.68	110,764.29	97,601.33 (−11.9%)	92,643.47 (−16.4%)
4000	20	50	0.9	167,525.18	159,496.52 (−4.8%)	142,004.99 (−15.2%)
5000	20	50	0.46	240,787.52	236,348.69 (−1.8%)	216,667.51 (−10.0%)
6000	20	50	0.00	355,593.19	355,593.19 (−0.0%)	338,487.15 (−4.8%)
3000	10	50	1.70	76,037.38	75,659.67 (−0.5%)	75,190.17 (−1.1%)
3000	50	50	3.71	193,161.06	175,207.07 (−9.3%)	132,660.51 (−31.3%)
3000	100	50	0.71	459,066.28	236,659.62 (-48%)	196,536.95 (−57.2%)
4000	20	25	1.09	204,915.79	171,403.84 (−16.4%)	148,326.00 (−27.6%)
4000	20	75	0.94	163,116.06	151,028.89 (−7.4%)	135,447.73 (−16.9%)
4000	20	100	0.50	160,953.39	153,999.99 (−4.3%)	128,888.20 (−19.9%)
4000	20	200	0.00	120,572.28	120,572.28 (−0.0%)	120,096.35 (−0.4%)

5.1.2. OCP results

Now we solve for OCP under different settings of total demand q^{16}, curb capacity κ and driving parking fee μ_s. Since the initial curb charge does not affect the optimized curb charge and negative charge (incentives for ride-hailing) is not allowed in our experiment, we always start from $\mathbf{m} = \mathbf{0}$. In the 6-link network, only link $1 \to 2$ and $5 \to 6$ have curbside PUDOs and these two links correspond to the start and end of the same set of paths, so the curb prices on these two paths will always be the same. Curb price on all other links has no effect on the 6-link network. Therefore, when presenting optimal curb price for 6-link network, we only show a single number, which is the curb price shared by link $1 \to 2$ and $5 \to 6$.

To evaluate the effectiveness of our OCP strategy, we compare the total social cost (TSC), in three scenarios of same setting: (1) without curb pricing, (2) with optimal curb pricing and (3) path-based system optimum (SO) without curb pricing. The TSC is calculated by the objective function in Eq. (20) with $f_{\text{penalty}}(x) = x$, as stated in Remark 3. We also calculate the corresponding TSC reduction by the implementation of OCP and path-based SO comparing with scenarios without curb pricing. The details about formulation and solution algorithm for path-based SO can be found in Appendix. The test results are summarized in Table 5.

When the demand is very high, the network and curb become heavily congested. Adding a curbside charge does not effectively reduce total social cost. When the curb is already terribly congested, discouraging a small amount of users from making a stop at the curb does not change the overall traffic flow as much. However, the curbside charge is most effective when it is able to reduce curbside queues in a way to substantially reduce travel time on links. In general, the OCP does not work very well for networks of heavy traffic but can be effective for moderate traffic volumes in the network.

In addition, the result shows that low curbside capacity contributes to heavy curb congestion. The OCP strategy can discourage ride-hailing travelers from accessing the curb to ensure curb spaces are used efficiently, ultimately reducing the social cost. But for the cases with sufficient curbside capacity already, there is little congestion at the curbside. Thus, adding additional curb charge does not help reduce total social cost as much. With varying driving parking fees, we see that OCP can be very effective when the parking fee is high. The more expensive driving parking is, the more preferable ride-hailing services are, leading to more congestion at the curb. Thus OCP strategy can effectively reduce the total social cost when parking fee is high, even the optimal curbside fee is very small. The optimal curbside fee is higher when the parking fee is moderate and market shares for both ride-hailing and driving are comparable, because more disincentives are needed to shift some travelers for driving to enjoy the full benefits of reducing curbside queuing.

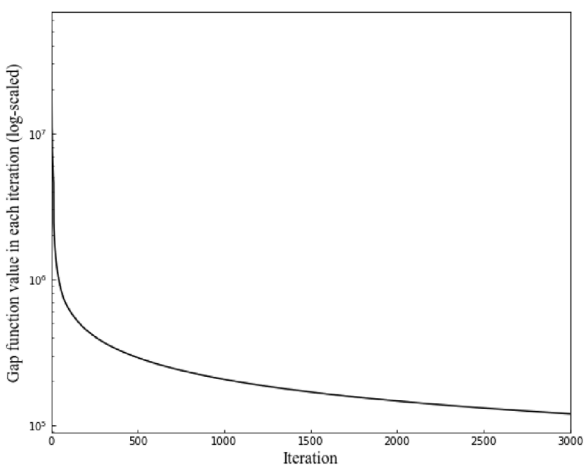

(a) BMUE convergence

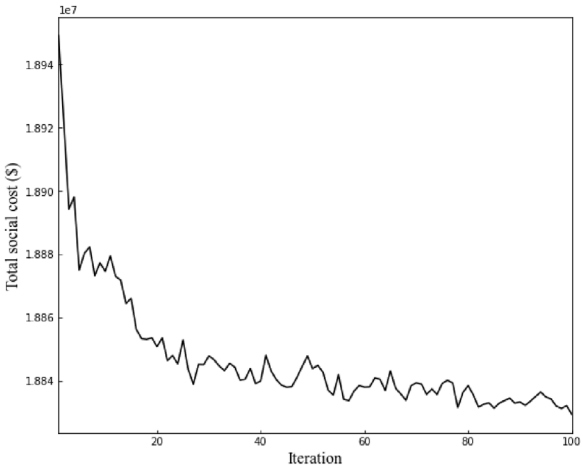

(b) OCP convergence

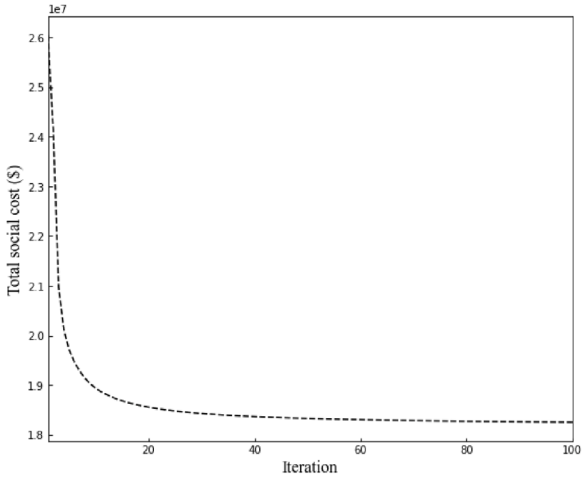

(c) Path-based SO Convergence

Fig. 6. Convergence performance for Sioux-Falls network.

5.2. Sioux-Falls network

We also use the Sioux-Falls network to test our method. Detailed network structure and demand can be found in Transportation Networks for Research Core Team (2021). The network settings are identical to Table 3, and the upper bound of curb price is set to $20 and no negative charge (incentives) is allowed as well. Fig. 6 shows the curves of convergence performance for BMUE without curb pricing, SA-based solution algorithm for optimal curb pricing, and path-based SO. It can be seen that in the convergence curve under OCP, the social cost fluctuates slightly over iterations and reduces quickly in the first 20 iterations. The fluctuation is caused by the sensitivity to equilibrium states of the SA algorithm and a chosen fixed learning rate. For Sioux-Falls network or larger network (to be presented later), stable convergence is relatively hard to achieve because the resulting magnitude of gradients over iteration can vary considerably, so the learning rate will have a great effect on the convergence performance. It is recommended to use normalized gradient descent to scale the gradient magnitude and use a relatively small learning rate. Also Adagrad algorithm (Duchi et al., 2011) is recommended which has a decaying learning rate with respect to gradient magnitude. Even though we use normalized gradients to update in each iteration, the total system cost is not guaranteed to drop in each iteration, but the overall performance is satisfactory in practice.

After implementing OCP, the network social cost reduces by 0.63%, down from $18,949,050.0 to $18,829,283.7 comparing to the total social cost under SO $18,251,743.6, down by 3.68% from the scenario without curb pricing. It means that the OCP could be 16.7% as effective as SO, provided with the demand pattern used in the literature Suwansirikul et al. (1987), Meng et al. (2001) and Wang et al. (2013).

In Section 3.1, we mentioned that the O-D demands are exogenous in our study and could be estimated based on planning models or real-world data. A big challenge of the OD estimation problem is that we need to estimate based on sparse and partial observations

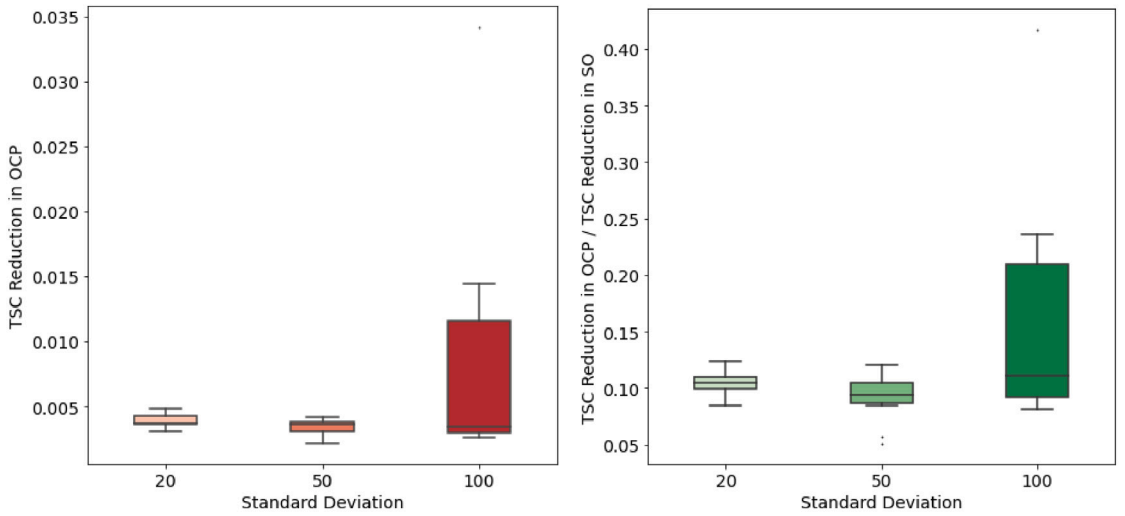

(a) TSC reductions with OCP

(b) TSC reduction with OCP/TSC reduction with SO

Fig. 7. Boxplots for testing OCP with varying demand estimation errors.

of the network, which inevitably results in biased estimation. In order to test the robustness of OCP to the biased estimations of OD demand, we introduce artificial errors to the "true" demand of Sioux-Falls network and examine how the effectiveness of OCP can be impacted by the demand estimation errors. The demand error terms are assumed to follow Gaussian distribution with zero mean and standard deviation (SD) of three values: 20, 50 and 100. For each SD, we draw ten groups of error samples and add them to the "true" demand, then compute OCP with respect to the new demand that is biased artificially. The total social cost reductions under OCP and the ratio between TSC reduction with OCP and SO, are shown respectively in Fig. 7. Each boxplot for the corresponding SD level contains ten test scenarios with the same setting but error terms are generated with different random seeds and added to the "true" demand matrices. One can see that the TSC reductions with OCP do not fluctuate as much when SD equals to 20 or 50. However, when SD increases drastically to 100, the TSC reduction has a distribution of a wider range, implying that OCP benefits varies substantially when the estimated demand is highly biased, but the overall effectiveness is still acceptable since the reductions tend to be greater in general. Therefore, our method can be robust to the demand estimation errors.

5.3. Pittsburgh Downtown network

We further test the proposed models in a real-world network in Pittsburgh Downtown area. As shown in Fig. 8, the origin nodes are denoted in green and destination nodes are denoted in red. The network parameters and model coefficients are shown in Table 6. In our setting, all destination nodes are in the downtown area, meaning all travelers in our model are heading to downtown in the morning commuting time period. The phase "demand" for this network refers to the demand of each O-D pair that shares an identical demand value for all O-D pairs.

5.3.1. Sensitivity analysis for BMUE

We first run the MSA algorithm to solve BMUE under the default settings of $\kappa = 50$ and $\mu_s = 20$ without curb pricing. The convergence performance for varying demand is shown in Fig. 9. As demand increases, MSA algorithm takes a longer time to converge if using the same step size; hence it is recommended to use a larger step size when demand is high. Next, we fix the demand as 200 veh/h and vary curb capacity and destination parking fee to analyze the sensitivity of BMUE solutions. The resulting heatmap is shown in Fig. 10. It demonstrates that without curbside pricing, more travelers would like to choose ride hailing when parking cost and curb capacity both increase. Both parking and curbside capacity are the two main factors influencing the choice of ride-hailing services.

5.3.2. OCP results

We calculate OCP under various network settings. The results are summarized in Table 7. Overall, the results of proposed OCP framework is satisfactory, and OCP seems promising in reducing social cost. For a fixed parking fee of $10 and curb capacity of 50 veh/mile, SO reduces TSC by around 20% and OCP can reduce TSC by around 6% when demand is 150. As demand increases, OCP strategy can become more effective, contributing to more TSC reductions. When demand is set 300 veh/h, the TSC reduction by OCP is 13.51%, most effectively comparing to the SO case (19.13%). Similar results can also be found under other settings. We conclude that for a large network, even in high demand case, the OCP may perform well to effectively reduce total social cost of the entire network.

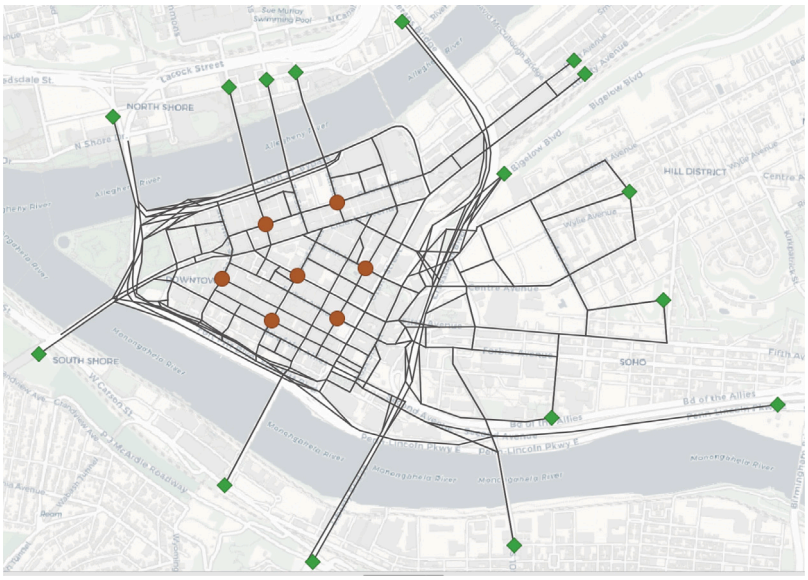

Fig. 8. An overview of the Pittsburgh downtown network. (For interpretation of the references to color in this figure legend, the reader is referred to the web version of this article.)

Table 6
Network parameters and model coefficients for Pittsburgh Downtown.

Name	Value
Number of links	573
Number of nodes	247
Number of origins	16
Number of destinations	7
Number of O-D pairs	112
Total commute duration T	60 min
Value of time constant α	0.1 $/min
The per mile unit cost constant for driving μ_m	0.5 $/mile
Average time for a vehicle to complete a curbside stop t_c	2 min
Constant for logit choice model α_D	1
Constant for logit choice model α_R	2
Constant for logit choice model β	1
Constant to regulate queuing model ϵ	0.01
Maximum path size for each O-D and each mode ξ	20
Maximum walking distance before pick-ups or after drop-offs ζ	0.2 mile
Curb price upper bound	10 $
Curb price lower bound	0 $
Default curb capacity κ	50 veh/mile
Default destination parking fee for driving μ_s	20 $
Walking speed	0.05 mile/min

When parking fee increases, the total social costs of cases without OCP and SO have larger discrepancies. This can be interpreted by that a large parking fee ($20, $50 and $100) would motivate travelers to choose ride-hailing services, and thus more pick-ups and drop-offs occur at the limited curb space, increasing curb congestion cost and total social cost comparing to SO. When we implement OCP, an upper bound for curb price ($10 in this case, smaller than parking fee in this case) is set. Therefore, the effectiveness of OCP may be limited. Similar observations can also be found in the cases of large curbside capacity. Especially for cases with curb capacity of 100 veh/mile and parking fee of 20$, TSC reductions under SO are the greatest (more than 40%) for varying demand settings, whereas TSC reduction under OCP are over 10%, also substantial, but not as effective as SO.

In the case of last row in Table 7 (demand = 200 veh/h, parking fee = $100, curb capacity = 100 veh/mile), the performance of OCP is poor, not good as other settings with a TSC reduction of less than 1%. In this case, both the parking cost for driving and curb capacity are large, implying that using private vehicles could have a high travel cost, but ride-hailing vehicles would not due to adequate curb spaces. Then ride-haling is much more attractive to travelers comparing to driving. Thus, imposing a relatively small curb fee (upper bounded by $10) would not be able to influence the mode choices as much to reduce TSC. The setting may not be ideal in practice since the parking fee is exaggerated, but it indeed shows that OCP has limited effectiveness depending on travel cost and infrastructure settings, particularly when the curbside charge has a ceiling too low to influence travelers' choices.

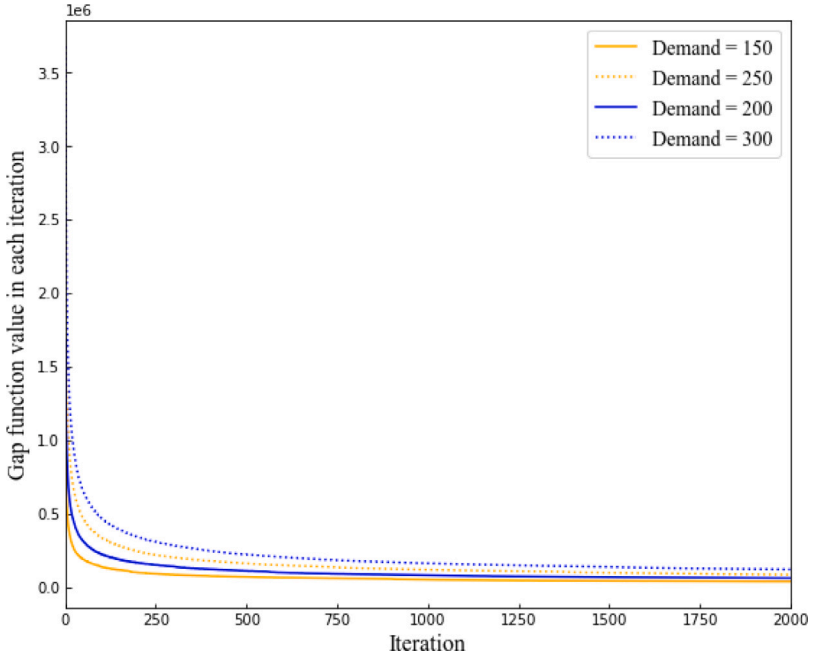

Fig. 9. MSA convergence for two demand settings.

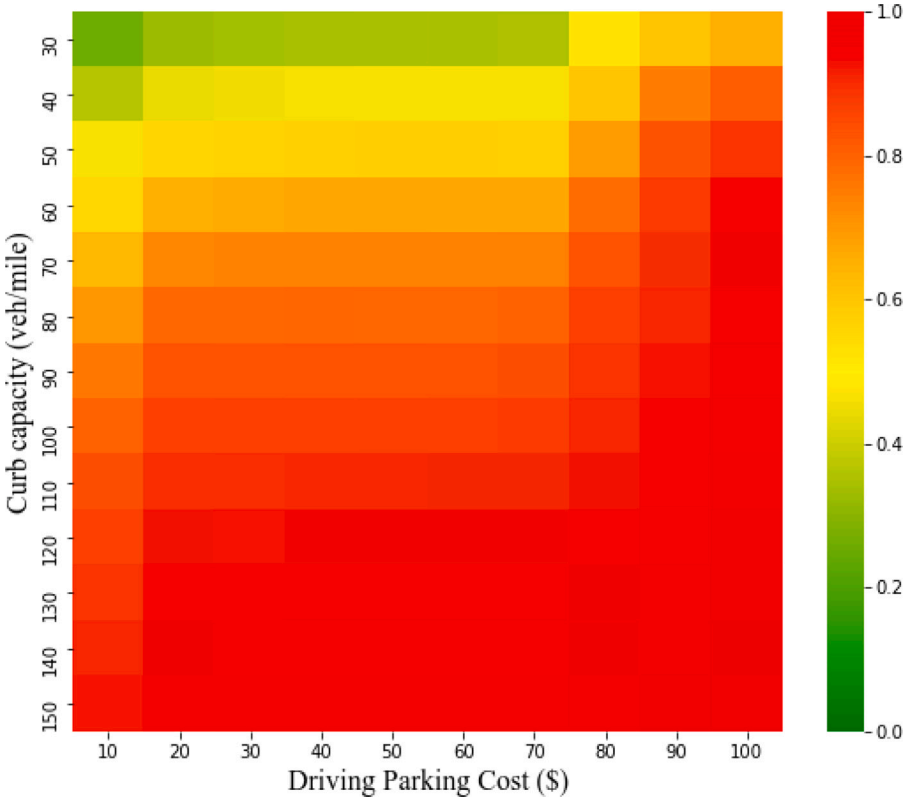

Fig. 10. Ride-hailing mode choice fraction in different settings.

Table 7
Total social cost in different settings.

O-D Demand (veh/h)	Parking fee ($)	Curb capacity (veh/mile)	Total social cost ($)		
			w/o pricing	w/ OCP (reduction)	SO (reduction)
150	10	50	179,436.74	168,817.98 (−5.92%)	138,090.19 (−20.04%)
200	10	50	252,831.77	228,468.45 (−9.64%)	198,040.28 (−21.67%)
250	10	50	325,116.94	296,682.71 (−8.75%)	258,222.72 (−20.58%)
300	10	50	394,011.89	340,767.25 (−13.51%)	318,619.31 (−19.13%)
150	20	50	365,913.81	318,763.54 (−12.89%)	231,011.43 (−36.87%)
200	20	50	508,604.85	451,335.41 (−11.26%)	347,590.03 (−31.66%)
250	20	50	650,201.24	576,480.89 (−11.34%)	540,532.79 (−28.78%)
300	20	50	789,728.85	706,547.97 (−10.53%)	578,993.28 (−26.68%)
150	20	100	234,654.76	208,311.43 (−11.23%)	133,766.03 (−42.99%)
200	20	100	433,741.66	369,878.94 (−14.72%)	225,432.26 (−48.03%)
250	20	100	609,955.15	530,629.52 (−13.01%)	335,551.81 (−44.99%)
300	20	100	784,261.14	671,184.68 (−14.42%)	450,740.60 (−42.53%)
200	10	50	252,831.77	228,468.45 (−9.64%)	198,040.28 (−21.67%)
200	50	50	1,079,087.36	1,001,931.60 (−7.15%)	776,953.61 (−28.00%)
200	100	50	1,415,061.61	1,340,088.43 (−5.30%)	1,048,332.94 (−25.92%)
200	10	100	211,201.58	203,167.42 (−3.80%)	152,090.58 (−27.99%)
200	50	100	789,827.30	749,708.80 (−5.08%)	527,887.41 (−33.16%)
200	100	100	875,482.47	868,179.87 (−0.83%)	627,501.87 (−28.33%)

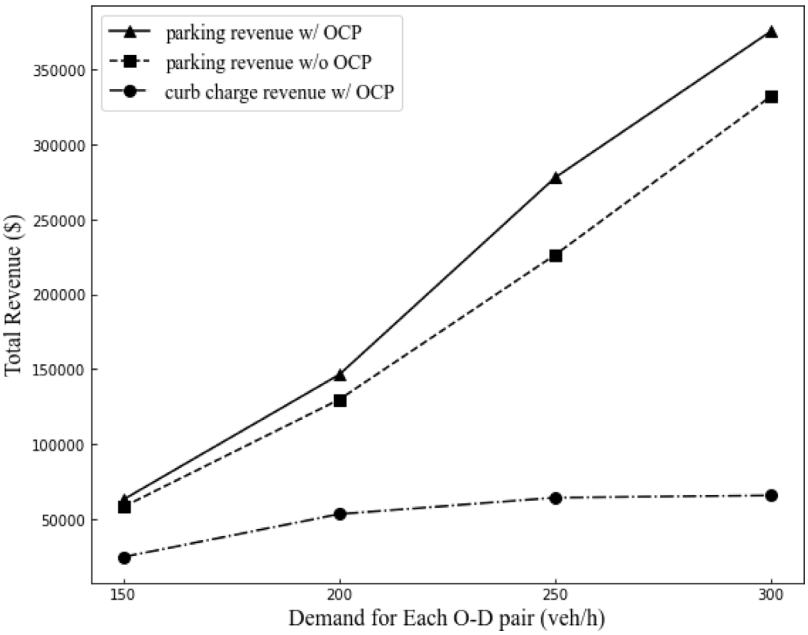

Fig. 11. Parking and curb charge revenue in different demand settings.

Fig. 11 shows the revenues from parking and curbside charge. It is intuitive that in different demand settings, parking revenues with OCP implementation are all higher than those without OCP since the OCP strategy increases the fraction of choosing private driving and consequently increase total parking revenues. Curb charge revenue increases with respect to total demand in general, but not so much when demand increases beyond a certain level. This implies that OCP does not intend to charge more when network becomes highly congested, rather, its goal is to balance curb resources in various locations to improve the overall network performance. Fig. 12 shows the heatmap of optimized curb prices under four demand scenarios. As can be seen, more congested network does not necessarily lead to higher curbside charges, re-ensuring OCP is very much location-based.

Fig. 13 compares travel costs under different demand settings. As demand increases, network becomes highly congested and apparently additional travel cost caused by curb congestion becomes greater resulting from more ride-hailing vehicles' stops. The figure also shows that after implementing the OCP, curb congestion is substantially alleviated, resulting in less travel cost caused by spillover queue at the curb. Meanwhile, OCP can also effectively reduce other travel costs, such as roadway congestion, by re-rerouting traffic flow, though the effect is not as pronounced as to reduce curb congestion. We further plot the heatmap of curb

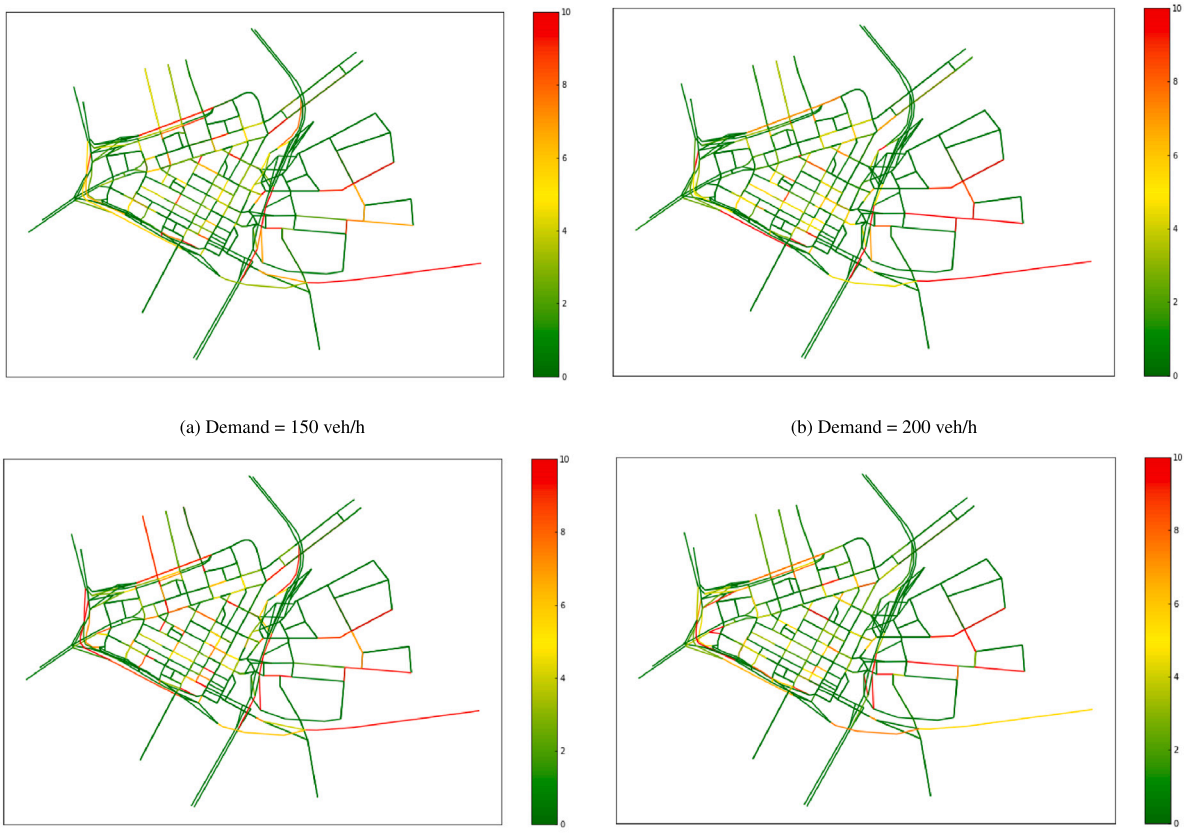

(a) Demand = 150 veh/h

(b) Demand = 200 veh/h

(c) Demand = 250 veh/h

(d) Demand = 300 veh/h

Fig. 12. Optimal Curb Pricing (OCP) heatmap for various demand scenarios.

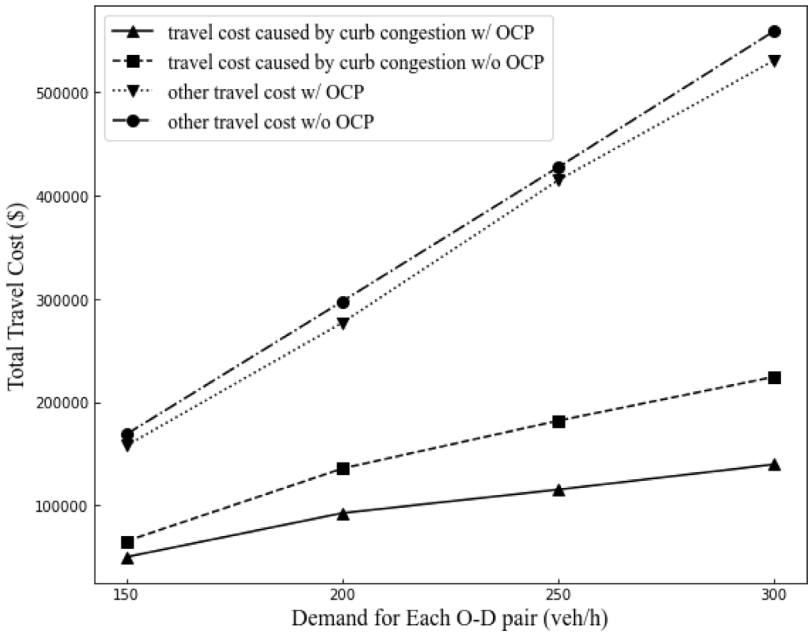

Fig. 13. Travel cost in different demand settings.

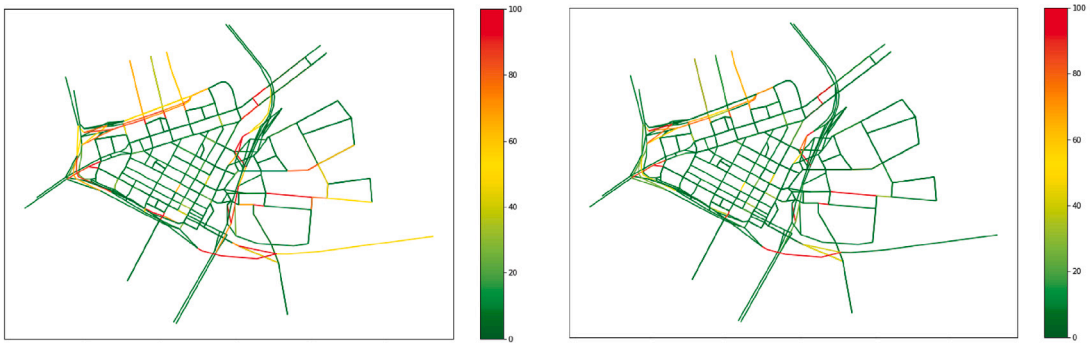

(a) before OCP (b) after OCP

Fig. 14. Before-after curb queue heatmap for demand = 150 scenario.

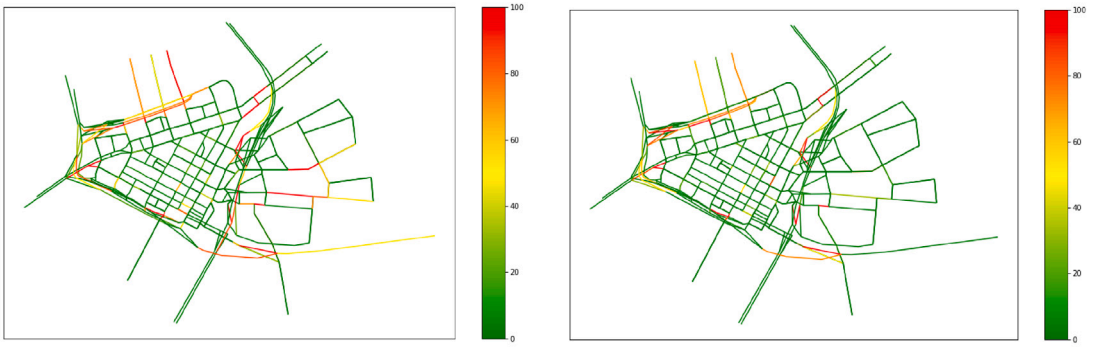

(a) before OCP (b) after OCP

Fig. 15. Before-after curb queue heatmap for demand = 200 scenario.

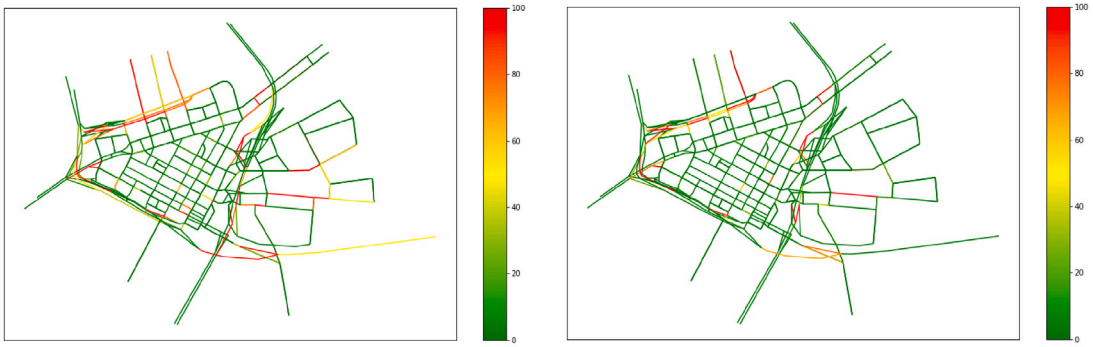

(a) before OCP (b) after OCP

Fig. 16. Before-after curb queue heatmap for demand = 250 scenario.

queue lengths for cases under different demands before and after implementing OCP (Figs. 14–17). The heatmaps are consistent with the results above, demonstrating that the OCP strategy can help reduce curb congestion and contribute to the reduction of network social cost. Fig. 18 confirms that OCP strategy can significantly reduce the average waiting time for all curb locations by more than 30%.

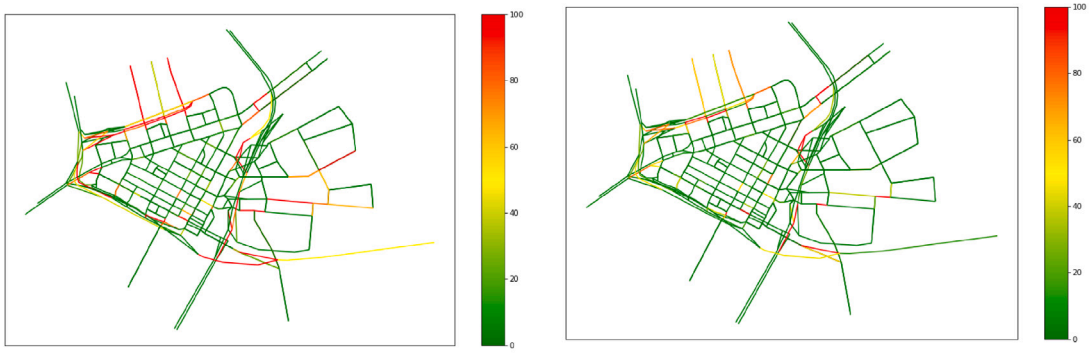

(a) before OCP (b) after OCP

Fig. 17. Before-after curb queue heatmap for demand = 300 scenario.

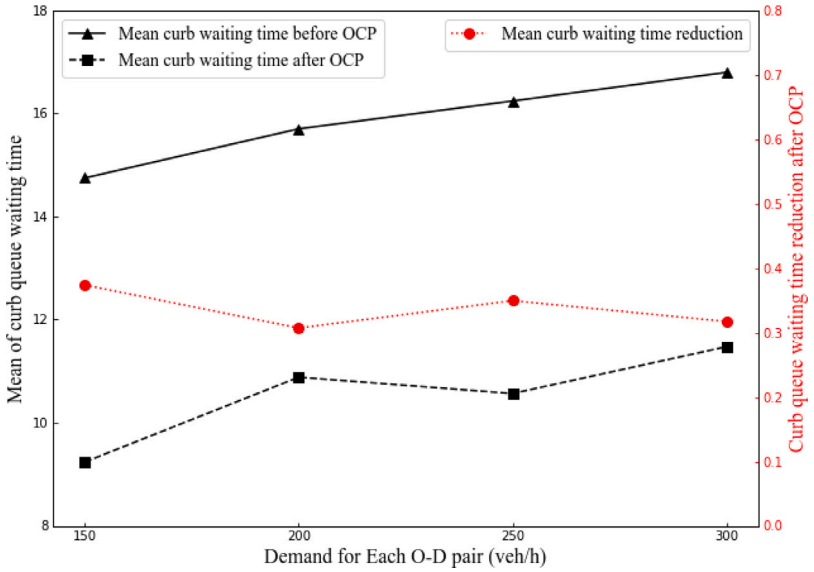

Fig. 18. Mean curb waiting time before and after OCP.

6. Conclusions

This paper studies the impact of curb utilization by ride-hailing service stops. The impact of curb stops could be tremendous, clogging both the curbs and driving lanes, influencing travelers' modal choices on ride-hailing or driving, among many other impacts to urban communities. We develop a network model integrating curb uses into classical traffic assignment models through a novel bi-modal user equilibrium (BMUE), and propose an optimal curb pricing strategy for managing pick-up/drop-offs of ride-hailing vehicles. The BMUE model considers both driving and ride-hailing modes competing for roads and curb spaces, and integrates a curbside queuing model to quantify the additional curb and driving lane congestion caused by ride-hailing pick-ups/drop-offs. The cost of curb use influences whether a traveler chooses ride-hailing or driving, and where a ride-hailing trip makes its stop near the respective destination. Therefore, travelers make joint choices of modes, curb pick-up and drop-off locations when using ride-hailing or parking locations when using private driving. The BMUE problem is cast into an equivalent variational inequality problem and a heuristic solution algorithm with column generation is developed to solve BMUE. To determine optimal curb prices, a bi-level optimization framework is developed with the object of minimizing total social cost, which is solved by a sensitivity analysis-based method.

The proposed methods are examined on a small toy network, Sioux-Falls network and Pittsburgh Downtown network. We also conduct sensitivity analysis of the optimal curbside pricing (OCP) with respect to various settings on demand and cost coefficients. Overall, the results are satisfactory and robust, demonstrating that the OCP strategy can alleviate curb congestion and reduce social cost effectively even when the network is large and congested. The curb-aware network models could help public agencies to better understand the impacts of ride-hailing pick-ups and drop-offs on curbside spaces, and provide policy implications for curbside

regulations. Meanwhile the OCP strategy would not have a substantial impact on other travel modes if set properly. Even better, it would actually reduce the travel cost potentially induced by the curb congestion, benefiting all travelers in the urban network.

Generally, the framework in our study should be able to accommodate other cases of curb use and management. For example, airport is an important application for curbside PUDO which has been widely studied. Travelers heading to or from an airport could have multiple modes (i.e., drive and park, public transit, shuttle, etc.) including ride-hailing. The mode choice may also follow a nested logit model. Similarly, curb queue model can be integrated into the utility function of each mode to solve for the network flow pattern considering curb usage. Differently, in an airport, curb spaces may be used exclusively by ride-hailing service vehicles and private vehicles, and drive and park users would use off-curb parking lots, meaning that parking and curb spaces are entirely separate, but it can be seen as a special case of our general network setting. The OCP can also be used to manage the curbside space aiming to influence the traffic flow, parking revenue and PUDO waiting time, etc.

On the long-term planning horizon, this paper studies the impact of curbside pricing for peak hours and proposes methods to derive optimal curbside prices that vary by location. Those location-specific curbside prices represent the expected average charge for each curb on the daily basis. In practice, they can be a base pricing for curbside management, in addition to pricing changes that aim for real-time or short-term management on the fly. Overall, OCP can be used for policy making and long-term strategic decision for infrastructure investment. For instance, curbs with a high optimal price can be identified as critical curbs to invest since high pricing indicates that, at the network level, these curbs are more likely to congest heavily. We can either prioritize deploying sensors in those critical curb spaces for management and pricing or invest on expanding those curb spaces to improve system-level performance. Additionally, public agency can use OCP as an indicator to build pooled PUDO locations for ride-hailing or other mobility services. It is also possible to identify optimal curbside pricing for different demand/supply scenarios using this modeling framework, such as under seasonal effects.

In the near future, we plan to extend this study in the following directions: (1) the framework can be extended to dynamic transportation networks to implement time-varying curb pricing considering dynamic travel demand and mode choices; (2) we can integrate additional travel modes (i.e. transit, ride-sharing) into the network flow model to better understand the impact of curbside management to all modes; (3) real-world multi-source data can be used to calibrate the model and explore more insights on curb management in practice. This paper uses synthetic data to consider the effects of curbside queuing model on through traffic, which could be further improved by using real-world ride-hailing vehicle trajectory data; and (4) a gradient-based method to determine the optimal curb prices could be computationally expensive for large networks. The computational efficiency can be further optimized to run on parallel computing architectures.

Acknowledgments

This research is supported by a National Science Foundation grant CMMI-1931827, and a Department of Energy grant DOE-EE0009659. The authors would like to thank Leo Huang who was a Research Assistant to provide some initial work on an earlier version of this work.

Appendix A. Path-based system optimum formulation

This appendix shows the formulation and solution algorithm of path-based system optimum (SO). The path-based SO problem with the same bi-modal setting is formulated as Eq. (41). The objective is to minimize the total social cost of the network and the constraint is the sum of path flows equals to O-D demand.

$$\begin{aligned} &\min \mathrm{TSC}(\mathbf{f}) = \mathbf{f} \cdot \mathbf{c}' \\ &\text{s.t.} \quad \mathbf{M}\mathbf{f} = \mathbf{q} \end{aligned} \tag{41}$$

The problem above can be formulated as a VI problem as Eq. (42).

$$\nabla_{\mathbf{f}} \mathrm{TSC}(\mathbf{f}^*)^{\top} (\mathbf{f} - \mathbf{f}^*) \geq 0, \quad \forall \mathbf{f} \in \Omega = \{\mathbf{f} : \mathbf{M}\mathbf{f} = \mathbf{q}\} \tag{42}$$

where Ω is the feasible set of $\mathbf{f}$, which is a polyhedron. The derivative of objective function with respect to $\mathbf{f}$ can be computed as Eq. (43).

$$\nabla_{\mathbf{f}} \mathrm{TSC}(\mathbf{f}) = \mathbf{c}' + \mathbf{f} \cdot \nabla_{\mathbf{f}} \mathbf{c}' = \mathbf{c}' + \mathbf{f} \cdot \nabla_{\mathbf{f}} \mathbf{c} \tag{43}$$

The computation of $\nabla_{\mathbf{f}} \mathbf{c}$ is in Eq. (36). The VI problem can be solve by the method of successive averages (MSA) shown in Algorithm 3. The step size in Algorithm 3 is diminishing as follows:

$$\lambda^{\nu} = \frac{1}{\nu + 1} \tag{44}$$

Algorithm 3: MSA algorithm for Path-based system optimum

Initialize path flow $\mathbf{f^0} \in \Omega$; $v = 0$ and λ^0;
repeat
  For all $(r, s) \in (R, S)$, compute the gradient $\nabla_{\mathbf{f}}\text{TSC}(\mathbf{f}^v)$ as derived in Equation (36) and (43) and find paths with the least gradient value for each rs, denoted by f_*^{rs};
  Generate an auxiliary path flow pattern $\mathbf{g}(\mathbf{f}^v)$ by assigning all demands of q^{rs} onto path f_*^{rs};
  Update path flow as $\mathbf{f}^{v+1} = (1 - \lambda^v)\mathbf{f} + \lambda^v\mathbf{g}(\mathbf{f}^v)$;
  Update λ^v to λ^{v+1}, $v = v + 1$;
until *Convergence criteria meets*;

Appendix B. Supplementary material

The proposed framework is implemented in Python and open-sourced on Github[1].

References

Abhishek, Legros, B., Fransoo, J.C., 2021. Performance evaluation of stochastic systems with dedicated delivery bays and general on-street parking. Transp. Sci. 55 (5), 1070–1087.

Acheampong, R.A., Siiba, A., Okyere, D.K., Tuffour, J.P., 2020. Mobility-on-demand: An empirical study of internet-based ride-hailing adoption factors, travel characteristics and mode substitution effects. Transp. Res. C 115, 102638.

Agarwal, S., Mani, D., Telang, R., 2019. The impact of ride-hailing services on congestion: Evidence from Indian cities. Available at SSRN 3410623.

Arnott, R., 2014. On the optimal target curbside parking occupancy rate. Econ. Transp. 3 (2), 133–144.

Arnott, R., Inci, E., 2006. An integrated model of downtown parking and traffic congestion. J. Urban Econ. 60 (3), 418–442.

Arnott, R., Inci, E., 2010. The stability of downtown parking and traffic congestion. J. Urban Econ. 68 (3), 260–276.

Arnott, R., Inci, E., Rowse, J., 2015. Downtown curbside parking capacity. J. Urban Econ. 86, 83–97.

Arnott, R., Rowse, J., 2013. Curbside parking time limits. Transp. Res. Part A: Policy Pract. 55, 89–110.

Ban, X.J., Dessouky, M., Pang, J.-S., Fan, R., 2019. A general equilibrium model for transportation systems with e-hailing services and flow congestion. Transp. Res. B 129, 273–304.

Battifarano, M., Qian, Z.S., 2019. Predicting real-time surge pricing of ride-sourcing companies. Transp. Res. C 107, 444–462.

Beojone, C.V., Geroliminis, N., 2021. On the inefficiency of ride-sourcing services towards urban congestion. Transp. Res. C 124, 102890.

Brown, A., 2022. Not all fees are created equal: Equity implications of ride-hail fee structures and revenues. Transp. Policy 125, 1–10, URL https://linkinghub.elsevier.com/retrieve/pii/S0967070X22001263.

Caleb, D., Andisheh, R., Anne, G., 2021. Curbspace management challenges and opportunities from public and private sector perspectives. Transp. Res. Rec.: J. Transp. Res. Board 2675 (2), 1413–1427.

Castiglione, J., Chang, T., Cooper, D., Hobson, J., Logan, W., Young, E., Charlton, B., Wilson, C., Mislove, A., Chen, L., et al., 2016. TNCs Today: A Profile of San Francisco Transportation Network Company Activity. Technical Report, San Francisco County Transportation Authority.

Castiglione, J., Cooper, D., Sana, B., Tischler, D., Chang, T., Erhardt, G.D., Roy, S., Chen, M., Mucci, A., 2018. TNCs & Congestion. Technical Report, San Francisco County Transportation Authority.

Castillo, E., Grande, Z., Calviño, A., Szeto, W., Lo, H., 2015. A state-of-the-art review of the sensor location, flow observability, estimation, and prediction problems in traffic networks. J. Sensors 2015, 1–26, URL: http://www.hindawi.com/journals/js/2015/903563/.

Chen, X., Di, X., 2021. Ridesharing user equilibrium with nodal matching cost and its implications for congestion tolling and platform pricing. Transp. Res. C 129, 103233.

Chen, Z., Xu, Z., Zangui, M., Yin, Y., 2016. Analysis of advanced management of curbside parking. Transp. Res. Rec. 2567, 57–66.

Chen, C., Yao, F., Mo, D., Zhu, J., Chen, X.M., 2021. Spatial-temporal pricing for ride-sourcing platform with reinforcement learning. Transp. Res. C 130, 103272.

Di, X., Ban, X.J., 2019. A unified equilibrium framework of new shared mobility systems. Transp. Res. B 129, 50–78.

Dowling, C.P., Ratliff, L.J., Zhang, B., 2020. Modeling curbside parking as a network of finite capacity queues. IEEE Trans. Intell. Transp. Syst. 21 (3), 1011–1022, URL https://ieeexplore.ieee.org/document/8663628/.

Duchi, J., Hazan, E., Singer, Y., 2011. Adaptive subgradient methods for online learning and stochastic optimization. J. Mach. Learn. Res. 12 (7).

Erhardt, G.D., Roy, S., Cooper, D., Sana, B., Chen, M., Castiglione, J., 2019. Do transportation network companies decrease or increase congestion? Sci. Adv. 5 (5), eaau2670, URL https://www.science.org/doi/10.1126/sciadv.aau2670.

Gao, J., Li, S., Yang, H., 2022. Shared parking for ride-sourcing platforms to reduce cruising traffic. Transp. Res. C 137, 103562.

Geroliminis, N., 2015. Cruising-for-parking in congested cities with an MFD representation. Econ. Transp. 4 (3), 156–165.

Goodchild, A., Mackenzie, D., Ranjbari, A., Machado, J., Chiara, G.D., 2019. Curb Allocation Change Project - Final Report. Technical Report, UNIVERSITY OF WASHINGTON.

Grahn, R., Qian, S., Matthews, H.S., Hendrickson, C., 2021. Are travelers substituting between transportation network companies (TNC) and public buses? A case study in Pittsburgh. Transportation 48 (2), 977–1005.

Guo, X., Caros, N.S., Zhao, J., 2021. Robust matching-integrated vehicle rebalancing in ride-hailing system with uncertain demand. Transp. Res. B 150, 161–189.

Guo, Z., McDonnell, S., 2013. Curb parking pricing for local residents: An exploration in New York City based on willingness to pay. Transp. Policy 30, 186–198.

He, F., Shen, Z.-J.M., 2015. Modeling taxi services with smartphone-based e-hailing applications. Transp. Res. C 58, 93–106.

Henao, A., Marshall, W.E., 2019. The impact of ride hailing on parking (and vice versa). J. Transp. Land Use 12 (1), URL https://www.jtlu.org/index.php/jtlu/article/view/1392.

Jones, E., Chatterjee, A., Marsili, R.L., 2009. A collaborative plan for curbside freight delivery in Washington, DC, USA. Inst. Transp. Eng. ITE J. 79 (5), 22–25.

Ke, J., Feng, S., Zhu, Z., Yang, H., Ye, J., 2021. Joint predictions of multi-modal ride-hailing demands: A deep multi-task multi-graph learning-based approach. Transp. Res. C 127, 103063, URL https://linkinghub.elsevier.com/retrieve/pii/S0968090X21000905.

Kontou, E., Garikapati, V., Hou, Y., 2020. Reducing ridesourcing empty vehicle travel with future travel demand prediction. Transp. Res. C 121, 102826.

Lei, C., Ouyang, Y., 2017. Dynamic pricing and reservation for intelligent urban parking management. Transp. Res. C 77, 226–244.

Li, Z., Hong, Y., Zhang, Z., 2016. Do ride-sharing services affect traffic congestion? An empirical study of uber entry. Soc. Sci. Res. Network 2002, 1–29.

[1] https://github.com/jiachaol/BMUE_TRC

Liu, W., Zhang, F., Yang, H., 2021. Modeling and managing the joint equilibrium of destination and parking choices under hybrid supply of curbside and shared parking. Transp. Res. C 130, 103301.
Ma, W., Pi, X., Qian, S., 2020. Estimating multi-class dynamic origin-destination demand through a forward-backward algorithm on computational graphs. Transp. Res. C 119, 102747, URL https://linkinghub.elsevier.com/retrieve/pii/S0968090X20306604.
Ma, W., Qian, Z.S., 2017. On the variance of recurrent traffic flow for statistical traffic assignment. Transp. Res. C 81, 57–82.
Ma, W., Qian, Z.S., 2018. Statistical inference of probabilistic origin-destination demand using day-to-day traffic data. Transp. Res. C 88, 227–256, URL https://linkinghub.elsevier.com/retrieve/pii/S0968090X17303765.
Mccormack, E., Goodchild, A., Sheth, M., Hurwitz, D., 2019. Developing design guidelines for commercial vehicle envelopes on urban streets. Int. J. Transp. Dev. Integr. 3 (2), 132–143.
Meng, Q., Yang, H., Bell, M., 2001. An equivalent continuously differentiable model and a locally convergent algorithm for the continuous network design problem. Transp. Res. B 35 (1), 83–105, URL https://linkinghub.elsevier.com/retrieve/pii/S0191261500000163.
Millard-Ball, A., Weinberger, R.R., Hampshire, R.C., 2014. Is the curb 80% full or 20% empty? Assessing the impacts of San Francisco's parking pricing experiment. Transp. Res. Part A: Policy Pract. 63, 76–92.
Nagurney, A., 2009. Variational Inequalities. Encyclopedia of Optimization. Springer, pp. 3989–3994.
Nair, G.S., Bhat, C.R., Batur, I., Pendyala, R.M., Lam, W.H., 2020. A model of deadheading trips and pick-up locations for ride-hailing service vehicles. Transp. Res. Part A: Policy Pract. 135, 289–308, URL https://linkinghub.elsevier.com/retrieve/pii/S0965856419310985.
Ni, L., Chen, C., Wang, X.C., Chen, X.M., 2021. Modeling network equilibrium of competitive ride-sourcing market with heterogeneous transportation network companies. Transp. Res. C 130, 103277.
Nourinejad, M., Ramezani, M., 2020. Ride-sourcing modeling and pricing in non-equilibrium two-sided markets. Transp. Res. B 132, 340–357.
Olus Inan, M., Inci, E., Robin Lindsey, C., 2019. Spillover parking. Transp. Res. B 125, 197–228.
Patkar, M., Dhamaniya, A., 2020. Developing capacity reduction factors for curbside bus stops under heterogeneous traffic conditions. Arab. J. Sci. Eng..
Pi, X., Ma, W., Qian, Z.S., 2019. A general formulation for multi-modal dynamic traffic assignment considering multi-class vehicles, public transit and parking. Transp. Res. C 104, 369–389.
Pu, Z., Li, Z., Ash, J., Zhu, W., Wang, Y., 2017. Evaluation of spatial heterogeneity in the sensitivity of on-street parking occupancy to price change. Transp. Res. C 77, 67–79.
Qian, Z.S., Rajagopal, R., 2014. Optimal dynamic parking pricing for morning commute considering expected cruising time. Transp. Res. C 48, 468–490.
Qin, G., Luo, Q., Yin, Y., Sun, J., Ye, J., 2021. Optimizing matching time intervals for ride-hailing services using reinforcement learning. Transp. Res. C 129, 103239, URL https://linkinghub.elsevier.com/retrieve/pii/S0968090X21002527.
Schimek, P., 2018. Bike lanes next to on-street parallel parking. Accid. Anal. Prev. 120, 74–82.
Shaheen, S., Cohen, A., Randolph, M., Farrar, E., Davis, R., Nichols, A., 2019. Shared Mobility Policy Playbook. Technical Report, Institute of Transportation Studies.
Sheffi, Y., 1985. Urban Transportation Networks: Equilibrium Analysis with Mathematical Programming Methods. Prentice-Hall, Inc., Englewood Cliffs, N.J. 07632, pp. 3989–3994.
Suwansirikul, C., Friesz, T.L., Tobin, R.L., 1987. Equilibrium decomposed optimization: A heuristic for the continuous equilibrium network design problem. Transp. Sci. 21 (4), 254–263, URL http://pubsonline.informs.org/doi/abs/10.1287/trsc.21.4.254.
Tirachini, A., Río, M.D., 2019. Ride-hailing in santiago de Chile: Users' characterisation and effects on travel behaviour. Transp. Policy 82, 46–57.
Tobin, R.L., Friesz, T.L., 1988. Sensitivity analysis for equilibrium network flow. Transp. Sci. 22 (4), 242–250.
Transportation Networks for Research Core Team, 2021. Transportation networks for research. https://github.com/bstabler/TransportationNetworks. (Accessed 21 July 2021).
Ugirumurera, J., Severino, J., Ficenec, K., Ge, Y., Wang, Q., Williams, L., Chae, J., Lunacek, M., Phillips, C., 2021. A modeling framework for designing and evaluating curbside traffic management policies at Dallas-Fort Worth International Airport. Transp. Res. Part A: Policy Pract. 153, 130–150, URL https://linkinghub.elsevier.com/retrieve/pii/S0965856421001956.
Urata, J., Xu, Z., Ke, J., Yin, Y., Wu, G., Yang, H., Ye, J., 2021. Learning ride-sourcing drivers' customer-searching behavior: A dynamic discrete choice approach. Transp. Res. C 130, 103293.
Wang, S., Meng, Q., Yang, H., 2013. Global optimization methods for the discrete network design problem. Transp. Res. B 50, 42–60, URL https://linkinghub.elsevier.com/retrieve/pii/S0191261513000179.
Wang, S., Noland, R.B., 2021. Variation in ride-hailing trips in Chengdu, China. Transp. Res. Part D: Transp. Environ. 90, 102596, URL https://linkinghub.elsevier.com/retrieve/pii/S1361920920307823.
Wang, X., Wang, J., Guo, L., Liu, W., Zhang, X., 2021. A convex programming approach for ridesharing user equilibrium under fixed driver/rider demand. Transp. Res. B 149, 33–51.
Wang, H., Yang, H., 2019. Ridesourcing systems: A framework and review. Transp. Res. B 129, 122–155, URL https://linkinghub.elsevier.com/retrieve/pii/S019126151831172X.
Wei, K., Vaze, V., Jacquillat, A., 2021. Transit planning optimization under ride-hailing competition and traffic congestion. Transp. Sci. trsc.2021.1068, URL http://pubsonline.informs.org/doi/10.1287/trsc.2021.1068.
Xu, Z., Chen, Z., Yin, Y., 2019. Equilibrium analysis of urban traffic networks with ride-sourcing services. Available at SSRN https://ssrn.com/abstract=3422294.
Xu, Z., Yin, Y., Chao, X., Zhu, H., Ye, J., 2021. A generalized fluid model of ride-hailing systems. Transp. Res. B 150, 587–605, URL https://linkinghub.elsevier.com/retrieve/pii/S0191261521000990.
Xu, Z., Yin, Y., Ye, J., 2020. On the supply curve of ride-hailing systems. Transp. Res. Part B 132, 29–43.
Yahia, C.N., Veciana, G.D., Boyles, S.D., Rahal, J.A., Stecklein, M., 2021. Book-ahead and supply management for ridesourcing platforms. Transp. Res. C 130, 103266.
Yang, H., 1997. Sensitivity analysis for the elastic-demand network equilibrium problem with applications. Transp. Res. B 31 (1), 55–70.
Ye, X., Yan, X., Chen, J., Wang, T., Yang, Z., 2018. Impact of curbside parking on bicycle lane capacity in Nanjing, China. Transp. Res. Rec. 2672 (31), 120–129.
Zha, L., Yin, Y., Yang, H., 2016. Economic analysis of ride-sourcing markets. Transp. Res. C 71, 249–266.
Zheng, N., Geroliminis, N., 2016. Modeling and optimization of multimodal urban networks with limited parking and dynamic pricing. Transp. Res. B 83, 36–58.
Zhu, P., Sirmatel, I.I., Trecate, G.F., Geroliminis, N., 2022. Idle-vehicle rebalancing coverage control for ride-sourcing systems. In: 2022 European Control Conference. ECC, IEEE, pp. 1970–1975.
Zimbabwe, S., 2018. RapidRide Roosevelt Corridor Curb Space Management Study. Technical Report, Seattle Department of Transportation.